

Water Resources Research

RESEARCH ARTICLE

10.1002/2014WR016509

Key Points:

- Distinct seasonal patterns of HR were observed across different climates
- HR fluxes are controlled by interplay between precipitation and transpiration
- Root hydraulic conductivities impact HR and transpiration differently

Supporting Information:

- Supporting Information: S1.

Correspondence to:

P. Kumar,
kumar1@illinois.edu

Citation:

Quijano, J. C., and P. Kumar (2015), Numerical simulations of hydraulic redistribution across climates: The role of the root hydraulic conductivities, *Water Resour. Res.*, 51, 8529–8550, doi:10.1002/2014WR016509.

Received 8 OCT 2014

Accepted 29 AUG 2015

Accepted article online 4 SEP 2015

Published online 29 OCT 2015

Numerical simulations of hydraulic redistribution across climates: The role of the root hydraulic conductivities

Juan C. Quijano¹ and Praveen Kumar^{1,2}

¹Department of Civil and Environmental Engineering, University of Illinois, Urbana, Illinois, USA, ²Department of Atmospheric Sciences, University of Illinois, Urbana, Illinois, USA

Abstract Hydraulic redistribution, a process by which vegetation roots redistribute soil moisture, has been recognized as an important mechanism impacting several processes that regulate plant water uptake, energy and water partitioning, and biogeochemical cycling. We analyze how the magnitude of hydraulic redistribution varies across ecosystems that are exposed to different climates and seasonal patterns of incoming shortwave radiation and precipitation. Numerical simulation studies are performed over 10 Ameriflux sites, which show that hydraulic redistribution predictions are significantly influenced by the specified root hydraulic conductivities. We performed sensitivity analyses by considering expected ranges of root conductivities based on previous experimental studies, and found contrasting patterns in energy-limited and water-limited ecosystems. In energy-limited ecosystems, there is a threshold above which high root conductivities enhance hydraulic redistribution with no increase in transpiration, while in water-limited ecosystems increase in root conductivities was always associated with enhancements in both transpiration and hydraulic redistribution. Further we found differences in the magnitude and seasonality of hydraulic redistribution and transpiration across different climates, regulated by interplay between precipitation and transpiration. The annual hydraulic redistribution to transpiration flux ratio (HR/Tr) was significant in Mediterranean climates ($HR/Tr \approx 30\%$), and in the tropical humid climates ($HR/Tr \approx 15\%$). However, in the continental climates hydraulic redistribution occurs only during sporadic precipitation events throughout the summer resulting in lower annual magnitudes ($HR/Tr < 5\%$). These results provide more insights for suitable implementation of numerical models to capture belowground processes in eco-hydrology, and enhance our understanding about the variability of hydraulic redistribution across different climates.

1. Introduction

The mechanism by which plant roots are able to transport moisture between soil layers by following gradients in water potential has been termed *hydraulic redistribution* (HR) [Burgess *et al.*, 1998, 2000, 2001; Hultine *et al.*, 2003, 2004]. Previous numerical and experimental studies have recognized that HR impacts several ecosystem processes such as transpiration (Tr) [Ryel *et al.*, 2002; Scott *et al.*, 2008; Amenu and Kumar, 2008], productivity [Dawson, 1993; Quijano *et al.*, 2012], ecological interactions [Dawson, 1993; Caldwell *et al.*, 1998; Quijano *et al.*, 2012; Wang *et al.*, 2011; Querejeta *et al.*, 2007], soil microbial dynamics [Querejeta *et al.*, 2003, 2007; Egerton-Warburton *et al.*, 2008], and decomposition and mineralization rates [de Kroon *et al.*, 1998; McCulley *et al.*, 2004; Aanderud and Richards, 2009; Armas *et al.*, 2011; Quijano *et al.*, 2013]. The potential to affect these ecosystem processes is mediated by the magnitude of the water fluxes associated with HR. However, the primary controls of these fluxes across climatic gradients remain unknown.

Although HR has been recognized as a process that is widespread [Caldwell *et al.*, 1998; Neumann and Cardon, 2012; Prieto *et al.*, 2012] and occurs across several plant species and climates, it has been mostly associated with ecosystems experiencing long dry periods where gradients in water potential are enhanced. Therefore, most of previous numerical and experimental studies have been performed in sites with extended dry periods that trigger HR fluxes, such as Mediterranean climates [Domec *et al.*, 2004; Warren *et al.*, 2008], the Amazonia [Oliveira *et al.*, 2005], or places that experience significant pulses of water such as Arizona in the US affected by the North American Monsoon [Scott *et al.*, 2008]. In contrast, it is expected that ecosystems with no prominent dry periods and more homogeneous distribution of rainfall throughout the year experience lower magnitude of HR fluxes. However, previous numerical efforts have focused in specific sites where significant fluxes of HR are expected. As a result, we still do not have a clear understanding

on how the magnitude of HR fluxes vary across ecosystems experiencing different patterns of precipitation (PPT).

We use a numerical model to analyze the magnitude and seasonality of HR fluxes across 10 Ameriflux sites located in ecosystems that are exposed to different climates. Our main goal is to analyze how the magnitude of HR varies across sites that are exposed to different patterns of shortwave (SW) radiation and precipitation. We implement the same modeling approach at all the sites and perform a common parameterization of all the above and belowground ecophysiological variables, including the root hydraulic conductivities. This numerical experiment provides a uniform basis for comparison and to assess the factors that control the magnitude of HR fluxes.

This paper is organized as follows: in section 2, we describe the model and in section 3 the study sites. In section 4, we show and discuss the results and validation of the simulations. In section 5, we analyze the seasonal dynamics of HR in different climates, and finally in section 6 we present the conclusions where we highlight the most important results and implications of this study.

2. Model Description

The ecohydrological dynamics are simulated with a previously published and validated model (MLCan) [Drewry *et al.*, 2010a,b; Quijano *et al.*, 2012; Le *et al.*, 2011, 2012]. Above the ground MLCan incorporates explicit coupling between leaf-level ecophysiological processes (photosynthesis and stomatal conductance), and physical processes (energy balance and boundary layer conductance). Among other variables, the model predicts the latent heat (LE) and sensible heat fluxes, and CO₂ fluxes (assimilation and respiration) through a detailed framework that incorporates an iterative solution of the leaf energy balance and photosynthesis. MLCan implements the Farquhar Model [Farquhar *et al.*, 1980] to simulate photosynthesis. Photosynthetic fluxes in C3 vegetation species in the Farquhar model are simulated with two main variables, the maximum carboxylation capacity (V_{cmax}) and the maximum rate of electron transport (J_{max}). Transpiration dynamics in MLCan are parameterized with the Ball-Berry (BB) model [Ball and Berry, 1982]. In the BB model, the stomatal conductance is simulated with two main variables, the BB slope (m) and the BB intercept (g). Parameters for each site that is simulated can be found in Table 1 and the sites are described in the next section.

Below the ground, the model uses the formulation developed by Mendel *et al.* [2002] and Amenu and Kumar [2008] to solve the coupled dynamics between roots and soil, including HR. This formulation resolves the flow in the roots by implementing a steady state approximation of the moisture dynamics in the roots that is coupled with the unsteady Richards Equation in the soil [Amenu and Kumar, 2008]: through the following equations:

$$\begin{aligned} \frac{\partial \theta}{\partial t} - \frac{\partial}{\partial z} \left[K_{soil} \left(\frac{\partial \psi_{soil}}{\partial z} - 1 \right) \right] &= -K_{e,rad} (\psi_{soil} - \psi_{root}) \\ - \frac{\partial}{\partial z} \left[K_{e,ax} \left(\frac{\partial \psi_{root}}{\partial z} - 1 \right) \right] &= K_{e,rad} (\psi_{soil} - \psi_{root}) \end{aligned} \quad (1)$$

where ψ_{soil} and ψ_{root} are the water potential in the soil and roots, respectively. The effective radial conductivity ($K_{e,rad}$) represents the capacity of the root system to transport water from the surrounding soil into the roots, while the effective axial conductivity ($K_{e,ax}$) refers to the capacity of the root system to transport water in the axial direction.

The distribution of root biomass is assumed to follow a logistic dose-response relation as suggested in Schenk and Jackson [2002]:

$$F_{root}(z) = \left[\frac{1}{1 + \left(\frac{z}{z_{50}} \right)^c} \right], \quad (2)$$

where $F_{root}(z)$ represents the cumulative fraction of root biomass that is above a depth z , z_{50} is the depth at which $F_{root}(z)=0.5$, and c is a dimensionless shape parameter that is function of z_{50} and z_{95} (depth at which $F_{root}(z)=0.95$). Values of z_{50} and z_{95} for the different ecosystems are presented in Table 1.

Table 1. Study Site Data^a

Sites	MET	BLO	HAR	HOW	MOR	WC	TAP	AC	DK
<i>General Information</i>									
Location	OR, USA	CA, USA	MA, USA	ME, USA	IN, USA	WI, USA	Para, Brazil	FL, USA	NK, USA
Long term MAP (mm)	400 ^b	1200 ^c	990 ^d	1000 ^d	1094 ^e	776 ^f	2000 ^g	1259 ^h	1140 ⁱ
Ameriflux MAP (mm)	492	1200	1138	810		751	1592	1000	
Tower height (m)	32	12.5	30	29	48	30	64	32	42
Canopy height (m)	22	6	23	20	27	24.2	45	24.4	25
Stand age (years)	60–90	16	80.5	109	70	55–90	Primary	80	90
<i>Information Used For Initial Conditions of Soil Moisture (SU: Spin-Up)</i>									
Initial Conditions	Data	Data	SU	SU	SU	Data	Data	SU	Data
Years spin-up			2000, 2001	2000, 2001	2000, 2001			2001	
Years simulation	2005–2006	2003–2004	2002–2003	2002–2003	2002–2003	2002–2003	2003–2004	2005	2004
<i>Aboveground Information</i>									
BB Slope (m) ^j	13	13	7	7	7	9	12	8	10
BB Intercept (g)(mol m ⁻² s ⁻¹)	0.001	0.001	0.001	0.001	0.001	0.001	0.001	0.001	0.001
V _{Cmax} (μmol m ⁻² s ⁻¹) ^{j,k,l}	70	V _t ^{m,n}	70	70	70	45	31 ^g	30	50
J _{max} (μmol m ⁻² s ⁻¹) ^{j,k,l}	120	V _t ^{m,n}	120	110	105	80	38 ^g	40	80
<i>Belowground Information</i>									
A _{basal} (m ² _{basal} ha ⁻¹)	32°	10 ^m	34 ^p	55 ^p	26 ^q	24 ^r	35 ^s	19 ^t	30 ^u
A _{ind,sa,coarse} (m ² _{root} m ⁻² _{ground}) ^y	9.2	2.4	9.7	15.2	7.6	7.0	10.0	5.3	8.5
A _{ind,sa,fine} (m ² _{root} m ⁻² _{ground}) ^w	6.7	6.7	6.0	6.4	5.7	5.7	8.4	6.5	7.6
A _{ind,sa} (m ² _{root} m ⁻² _{ground})	15.9	9.1	15.7	21.6	13.3	12.7	18.4	11.8	16.1
Root depth	7	7	3.0	2	3.5	3.0	10 ^x	2.5	2.0
z ₅₀ ^y (m)	0.4	0.4	0.2	0.2	0.2	0.2	1.2 ^x	0.2	0.15
z ₉₅ ^y (m)	2.4	2.4	1.3	0.8	1.3	1.0	5 ^x	1.1	0.4
Clay content ^o (%)	7	11	9 ^z	9	63	13	80 ^{aa}	85–30 ^{ab}	33–2 ^{ab}
Sand content ^o (%)	67	60	65 ^z	65	34	63	10 ^{aa}	4–40 ^{ab}	33–95 ^{ab}
Porosity (η) ^o	0.47	0.42	0.44	0.44	0.58	0.45–0.35 ^{ab}	0.57	0.4	0.53

^aSites: MET: Metolius Intermediate Pine, BLO: Blodget, HAR: Harvard Forest, HOW: Howland, MOR: Morgan-Monroe, WC: Willow Creek, TAP: Tapajós Km 67 and Tapajós Km 83, AC: Austin Cary, DK: Duke.

^bLaw et al. [1999].

^cMisson et al. [2006].

^dRichardson et al. [2009].

^eWayson et al. [2006].

^fCurtis et al. [2002].

^gDomingues et al. [2007].

^hPowell et al. [2005].

ⁱOren et al. [1998].

^jWullschleger [1993].

^kMedlyn et al. [1999].

^lCalibrated with data.

^mPereira de Carvalho et al. [2004].

ⁿV_t Vary in time.

^oFrom Ameriflux Network.

^pZhao et al. [2011].

^qSchmid et al. [2000].

^rEwers et al. [2008].

^sBaker et al. [2004].

^tPowell et al. [2008].

^uChristensen and Peet [1984].

^vCalculated.

^wJackson et al. [1997].

^xInferred from Oliveira et al. [2005].

^ySchenk and Jackson [2002].

^zMcFarlane et al. [2013].

^{aa}Pereira de Carvalho et al. [2004].

^{ab}V_s Vary in space.

2.1. Root Conductivities

As shown in equation (1), the HR dynamics is dependent on: (i) axial conductivity and (ii) radial conductivity [Frensch and Steudle, 1989; Melchior and Steudle, 1993; Tyree and Zimmermann, 2002; Huang and Nobel, 1994]. Information of root hydraulic conductivities is scarce and is available only for some vegetation species [Huang and Nobel, 1994; Tyree and Zimmermann, 2002]. In addition, root conductivities are usually measured in controlled experiments on isolated roots. In order to use this information in numerical or analytical models that simulate processes at the whole-plant scale, we must scale these properties from isolated

roots to the whole-plant level. We now present a formulation to scale conductivities measured in isolated roots in order to estimate the conductivity of the whole root system.

2.2. Radial Root Conductivity

Specific root radial conductivities K_{srad} ($\text{m}^3 \text{s}^{-1} \text{m}_{\text{root,sa}}^{-2} \text{ MPa}^{-1}$) is the root radial conductivity per unit surface of root area, and it refers to the discharge of water per unit area of root under a given water potential gradient between soil and root. For a constant water potential gradient between the soil and the root (ΔP_{sr}), at a depth z the total discharge ($Q_{\text{root,rad}}$) from the soil to the root is:

$$Q_{\text{root,rad}}(z) = K_{\text{srad}}(z) A_{\text{root,sa}}(z) \Delta P_{\text{sr}}(z), \quad (3)$$

where $A_{\text{root,sa}}$ ($\text{m}^2_{\text{root,sa}}$) is the total surface area of roots. Here we use the symbol P to indicate water potential in MPa units. Defining root surface area index $A_{\text{ind,sa}}$ ($\text{m}^2_{\text{root,sa}}/\text{m}^2_{\text{ground}}$) as the ratio between the root surface area and the ground surface area, we can compute the discharge from the soil to the root per unit of ground area at a given depth z as:

$$\begin{aligned} q_{\text{root,rad}}(z) &= \frac{Q_{\text{root,rad}}(z)}{A_{\text{ground}}} \\ &= \underbrace{\left[\frac{K_{\text{srad}}(z)}{\text{m}^3/\text{s}} \right]}_{\left[\frac{\text{m}^3/\text{s}}{\text{m}^2_{\text{root,sa}} \text{ MPa}} \right]} \underbrace{\left[\frac{A_{\text{ind,sa}}(z)}{\text{m}^2_{\text{root,sa}}} \right]}_{\left[\frac{\text{m}^2_{\text{root,sa}}}{\text{m}^2_{\text{ground}}} \right]} \underbrace{\left[\frac{\Delta P_{\text{sr}}(z)}{\text{MPa}} \right]}_{\left[\frac{\text{m}^3/\text{s}}{\text{m}^2_{\text{ground}}} \right]}. \end{aligned} \quad (4)$$

We define an effective root radial conductivity as:

$$K_{\text{e,rad}}(z) = K_{\text{srad}}(z) A_{\text{ind,sa}}(z) \frac{\rho g}{\Delta z}, \quad (5)$$

where Δz is a length scale in the vertical domain over which the flux of water between the root and the soil takes place, ρ is the water density, and g is the gravitational acceleration. Note that $K_{\text{e,rad}}$ has units of [time $^{-1}$ length $^{-1}$]. Therefore, the flux of water between the roots and the soil can be computed using $K_{\text{e,rad}}$ as:

$$q_{\text{root,rad}}(z) = K_{\text{e,rad}}(z) \Delta \psi_{\text{sr}}(z) \Delta z, \quad (6)$$

where $\Delta \psi_{\text{sr}} = (\psi_s - \psi_r)$ is the differential of water potential (in length units) between the soil and the roots. The soil moisture change due to the radial flux is then given by $K_{\text{e,rad}}(z) \Delta \psi_{\text{sr}}$ (as in equation (1)). Appendix A shows the formulation we are implementing to provide an estimation of $A_{\text{ind,sa}}$.

2.3. Axial Root Conductivity

Experiments conducted to measure the axial conductivity of roots are performed on isolated roots that have a particular radius r_r and length l_r under controlled gradients of water potential [Frensch and Steudle, 1989; Melchior and Steudle, 1993]. These experiments determine the discharge transported by the root when exposed to a fixed water potential difference. The discharge along the root occurring during the experiment is given as:

$$Q_{\text{root,ax}} = \left[\frac{\Delta P_{rr}}{l_r} \right] K_{\text{ax}}. \quad (7)$$

In this equation, ΔP_{rr} (MPa) is the water potential difference along the root system, l_r (m) is the root length used in the experiment, $Q_{\text{root,ax}}$ (m^3/s) is the experimental discharge, and K_{ax} ($\text{m}^4/\text{MPa}/\text{s}$) is the root axial conductivity. If all the conditions in the experiment are controlled, the discharge $Q_{\text{root,ax}}$, the difference in potential ΔP_{rr} , and the length of the root l_r are known. Based on this information, it is possible to obtain the conductivity of the root K_{ax} using equation:

$$K_{\text{ax}} = \left[\frac{Q_{\text{root,ax}}}{\Delta P_{rr}/l_r} \right]. \quad (8)$$

It is very common to report the axial conductivity per unit of root cross section $A_{\text{root,cs}}$:

$$K_{sax} = \frac{K_{ax}}{A_{root,cs}}. \quad (9)$$

This ratio K_{sax} ($\text{m}^4/\text{MPa}/\text{s}/\text{m}^2_{root,cs}$) is known as the *specific axial root conductivity* and provides a measure of how efficient the root is for transporting water in the axial direction per unit of root cross-sectional area. The water flux per unit of root cross-sectional area in a given isolated root where measurements have been performed is then given by [Tyree and Zimmermann, 2002]:

$$q_{isolated,ax} = - \frac{\partial(P_r + \rho g z)}{\partial l_r} K_{sax}. \quad (10)$$

We define the effective axial conductivity as the capacity of the root system to transport water in the axial direction at a given depth. At a particular depth, several roots of different diameters work in parallel to transport water. Therefore, the net conductivity at that depth can be computed as the sum of all the individual conductivities from the roots that are present at that depth:

$$K_{net,ax}(z) = \sum_i^{N_i} K_{ax,i}(z) = \sum_i^{N_i} K_{sax,i}(z) A_{root,cs,i}(z). \quad (11)$$

Assuming that K_{sax} remains constant for the entire root system:

$$K_{net,ax}(z) = K_{sax} \sum_i^{N_i} A_{root,cs,i}(z). \quad (12)$$

The net conductivity per unit of ground area can be defined as:

$$K_{gnet,ax}(z) = \frac{K_{net,ax}(z)}{A_{ground}} = \underbrace{\frac{K_{sax}}{\left[\frac{m^4}{m^2 \cdot \text{root},cs}\right]}}_{\left[\frac{m^4/\text{s}/\text{MPa}}{m^2 \cdot \text{root},cs}\right]} \underbrace{\left[\frac{A_{ind,cs}(z)}{\left[\frac{m^2}{m^2 \cdot \text{ground}}\right]}\right]}_{\left[\frac{m^3/\text{s}/\text{MPa}}{m^2 \cdot \text{ground}}\right]}, \quad (13)$$

where $A_{ind,cs}(z)$ is the root cross area index and represents the total cross-sectional area working in parallel at a given depth (z) per unit of ground area (Figure 1). Note K_{sax} is a representative specific axial conductivity for the root system and is obtained through measurements on isolated roots. Therefore, the discharge per unit ground area in the axial direction for the entire root system at a given depth is given as:

$$q_{roots,ax}(z) = - \underbrace{\frac{K_{gnet,ax}(z)}{\left[\frac{m^4/\text{s}/\text{MPa}}{m^2 \cdot \text{ground}}\right]}}_{\left[\frac{m^3/\text{s}}{m^2 \cdot \text{ground}}\right]} \left(\underbrace{\frac{\partial P_r(z) + \rho g z}{\partial l_r}}_{\left[\frac{\text{MPa}}{\text{m}}\right]} \right). \quad (14)$$

It is possible to define a factor f_{lz} as the rate of change of the mean root length with respect to z as:

$$f_{lz} = \frac{\partial \bar{l}_r}{\partial z} \approx \frac{\overline{L_{path}}}{\Delta z}, \quad (15)$$

where $\overline{L_{path}}$ is the mean root length in a soil of portion of thickness Δz . Multiplying both numerator and denominator in equation (14) by f_{lz} , it is possible to express $q_{roots,ax}$ in terms of z instead of l_r :

$$Q_{root,ax}(z) = \left[-K_{gnet,ax}(z) \left(\frac{\partial P_r(z)}{\partial l_r} + \frac{\partial(\rho g z)}{\partial l_r} \right) \right] \frac{f_{lz}}{f_{lz}}; f_{lz} > 0, \quad (16)$$

$$q_{roots,ax}(z) = \left[- \left\{ \frac{K_{gnet,ax}(z)}{f_{lz}} \right\} \left(\frac{\partial P_r(z)}{\partial z} + \frac{\partial(\rho g z)}{\partial z} \right) \right]. \quad (17)$$

Assuming constant water density and defining an effective axial conductivity as:

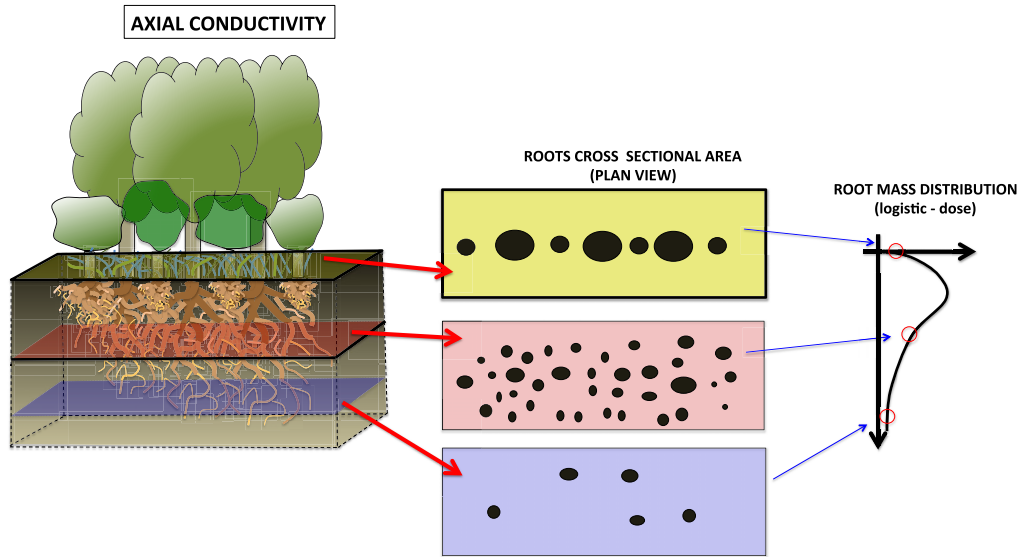


Figure 1. Schematic representation of the root cross-sectional area per unit of ground area ($A_{ind,cs}$) utilized to compute the effective root axial conductivity ($K_{e,ax}$). The total root surface area per unit ground area $A_{ind,cs}$ at the soil surface is inferred from the basal area reported at each site. The cross-sectional area at different depths is computed by assuming that $A_{ind,cs}$ has the same distribution as the root biomass (equation (2)).

$$K_{e,ax} = \frac{K_{gnet,ax}(z)\rho g}{f_{lz}}, \quad (18)$$

we obtain

$$q_{roots,ax}(z) = \left[-K_{e,ax} \left(\frac{\partial \psi_r(z)}{\partial z} + 1 \right) \right]. \quad (19)$$

Appendix B shows the formulation we are implementing to provide an estimation of $A_{ind,cs}$.

We estimated HR using equations (6) and (19) whenever $q_{root,rad}$ occurs from the root toward the soil. The fluxes of HR are decomposed in two components: (i) hydraulic lift (HL) which is the transport of moisture from deep to shallow layers during dry periods [Dawson, 1993; Espeleta et al., 2004; Ishikawa and Bledsoe, 2000; Ludwig et al., 2003]; and (ii) hydraulic descent (HD) which is the transport of moisture from shallow to deeper layers in the soil column during wet periods [Burgess et al., 1998; Schulze et al., 1998; Smith et al., 1999; Hultine et al., 2003]. The total flux of HR is given as $HR = HL + HD$.

2.4. Variation of Root Hydraulic Conductivities

In this study, root biomass is assumed constant throughout the year. However, specific root radial hydraulic conductivity is function of soil moisture, and therefore it changes with time following the soil moisture dynamics. As soil moisture departs from saturated conditions, K_{srad} decreases. We use the approximation suggested by Amenu and Kumar [2008] to account for the effect of soil water potential on root conductivities. Based on this formulation:

$$K_{srad}(\psi_{soil}) = \left(\frac{\psi_{soil}}{\psi_{soil,sat}} \right)^{-1/b} K_{srad}^s, \quad (20)$$

where K_{srad}^s is the specific radial hydraulic conductivity under saturated soil conditions, b is an empirical parameter suggested by Clapp and Hornberger [1978] that varies with the type of soil, and $\psi_{soil,sat}$ is the soil water potential at saturation. $K_{srad}(\psi_{soil})$ is the specific radial hydraulic conductivity as a function of soil water potential ψ_{soil} . This approximation captures the general pattern observed in previous studies [Nobel et al., 1990; Lopez and Nobel, 1991; Huang and Nobel, 1994; Domec et al., 2004] and it represents a consistent approach to compare sites with different soil types under a general assumption that root conductivity reduces with soil moisture.

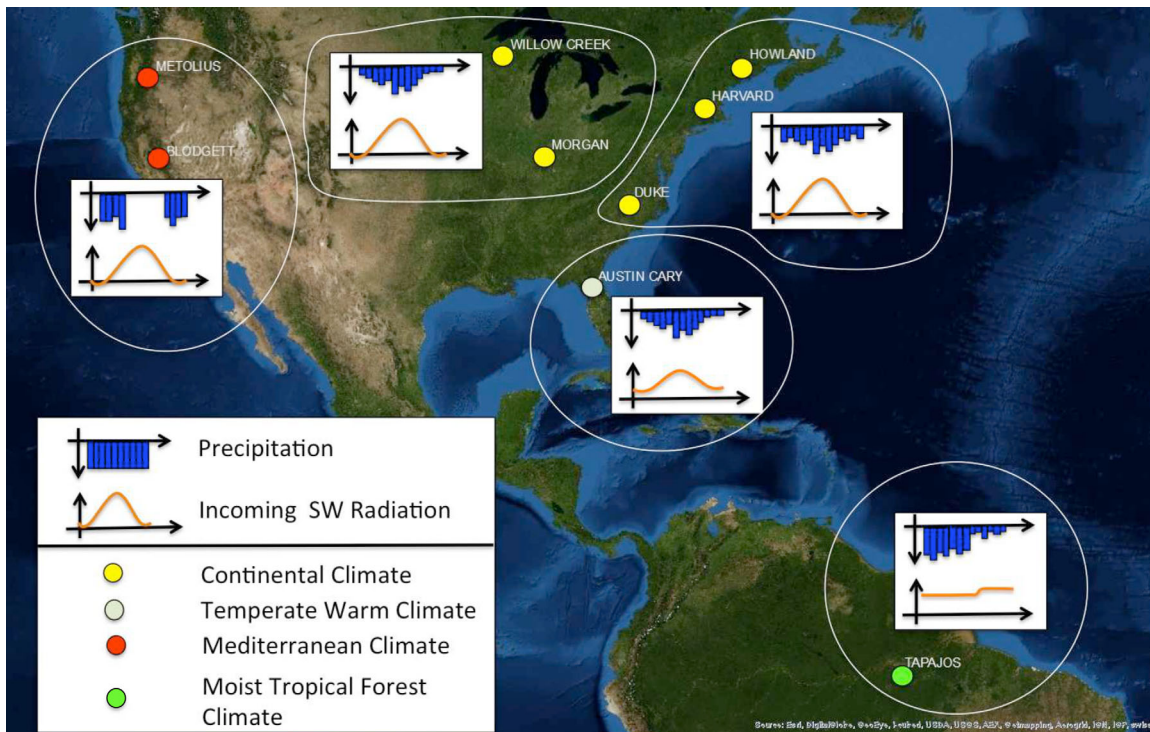


Figure 2. Geographic location of the 10 Ameriflux sites (same location is shown for Tapajós Km 83 and Tapajós Km 67) whose data were used in this study. The inset figures show a schematic representation of the annual patterns of precipitation and incoming SW radiation for each site. The circles surrounding the sites identify those sites with similar patterns of precipitation and shortwave radiation (see also Table 1).

3. Study Sites

The simulations were performed using forcing data from 10 Ameriflux towers. The ecosystems at these different Ameriflux sites exhibit a wide range of seasonal variability of rainfall and incoming SW radiation. The location of the sites is displayed in Figure 2, and the related information about these sites is presented in Table 1. Also supporting information Figure S1 shows the leaf area index for all the sites and years implemented in this study, and supporting information Table S1 shows the dominant species at each of these sites.

Two of the sites, *Metolius Intermediate Pine* (Metolius) and *Blodgett Forest* (Blodgett), experience a Mediterranean climate with dry summers and wet winters. The most prominent over-story species in these sites is *Pinus ponderosa*. Although these sites exhibit similar patterns in climate, the mean annual precipitation (MAP) is significantly higher in Blodgett Forest (Table 1).

Five other sites, *Harvard Forest* (Harvard), *Howland Forest* (Howland), *Willow Creek*, *Morgan-Monroe State Forest* (Morgan), and *Duke Forrest Hardwoods* (Duke) receive precipitation that is distributed throughout the year with lower values during the winter months and humid summers, and a clear seasonal variation of incoming SW radiation. Specifically, the climate in Duke presents warm summers, the climate in Howland and Morgan are considered as temperate continental with sharp annual variations in temperature, and that in Willow Creek is considered as northern continental with short growing season.

The *Austin Cary* site experiences a temperate warm climate with dry and mild winters and humid summers. Although precipitation is distributed throughout the year, it is higher between June and October. Also, the seasonality of incoming SW radiation is not as prominent as the other temperate ecosystems.

The *Tapajós Km 67* and *Tapajós Km 83* sites experience a tropical moist climate with a more homogenous annual distribution of SW radiation throughout the year and a higher mean annual precipitation (≈ 2000 mm) than the other sites that are considered in this study. These sites also experience a strong dry season between July and November. The reduction in precipitation during the dry season generates a strong variation in other variables such as incoming SW radiation, temperature, and humidity.

Table 2. Different Combinations of Specific Root Hydraulic Conductivities Used in This Study

ROOT SPECIFIC CONDUCTIVITIES			
Combinations	K_{srad}^s	K_{sax}	Conductivities
C1	1	1	$[m^3 \text{ MPa}^{-1} s^{-1} m_{\text{root,sa}}^{-2}]$
C2	2	1	10^{-9}
C3	3	1	10^{-8}
C4	4	1	10^{-7}
C5	1	2	10^{-6}
C6	2	2	
C7	3	2	
C8	4	2	K_{sax} Magnitude
C9	1	3	$(m^4 \text{ MPa}^{-1} s^{-1} m_{\text{root,cs}}^{-2})$
C10	2	3	10^{-4}
C11	3	3	10^{-3}
C12	4	3	10^{-2}
C13	1	4	10^{-1}
C14	2	4	10^0
C15	3	4	
C16	4	4	
C17	1	5	
C18	2	5	
C19	3	5	
C20	4	5	

available information of root biomass, densities, and structure below the ground is challenging to assess. Therefore, both root areas (biomass) and root conductivities represent the most prominent source of uncertainty in the model. Here we perform a sensitivity analysis of how specific root conductivities K_{sax} , and K_{srad}^s (see equations (9) and (20)) influence the water fluxes at the different sites. Note that K_{sax} and K_{srad}^s refer to axial and radial conductivities per unit of root surface area and cross-sectional area, respectively. Therefore, this sensitivity analysis implicitly involves the uncertainty associated with both root conductivities and root areas. We consider 20 different combinations (C1–C20) of K_{srad}^s and K_{sax} (see Table 2). Previous studies have found K_{srad}^s from 10^{-7} to 10^{-8} ($m^3 \text{ MPa}^{-1} s^{-1} m_{\text{root,sa}}^{-2}$) [Miyamoto et al., 2001; Huang and Nobel, 1994]. However, these values may change with vegetation type, and additional factors such as the rhizosphere conductivity, and mycorrhizae connections may reduce or enhance this conductivity, respectively. Therefore, we allow K_{srad}^s to vary from 10^{-9} to 10^{-6} ($m^3 \text{ MPa}^{-1} s^{-1} m_{\text{root,sa}}^{-2}$). We also allowed K_{sax} to vary from 10^{-4} to 10^0 ($m^4 \text{ MPa}^{-1} s^{-1} m_{\text{root,cs}}^{-2}$). These numbers comprise the range of values that have been reported in previous studies for K_{sax} [Huang and Nobel, 1994; Tyree and Zimmermann, 2002].

Figure 3 display total annual fluxes of Tr, HR, HD, HL, and gross primary production (GPP) for all the different combinations of K_{srad}^s and K_{sax} , for Metolius and Tapajós Km 83 sites. The left plots in Figure 3 show surface plots of HR and Tr for the entire set of combinations of specific conductivities that are considered. Note that HR, Tr, and GPP are affected by K_{srad}^s and K_{sax} . All HR, HD, HL, Tr, and GPP increase as the specific hydraulic conductivities increase. In particular, there is a high sensitivity of HR fluxes to K_{srad}^s . In all the sites, higher K_{srad}^s are always associated with higher HR. Therefore, we observe significant fluxes of HR for combination C20 in all the sites. This suggests that the magnitude of HR simulated by the model is highly sensitive to the specific root conductivities that are chosen. Figures for all the other sites are shown in supporting information Figures S2 and S3.

Although K_{srad}^s and K_{sax} impacts HR, Tr, and GPP, the effects vary across the different sites. We observe two main patterns:

1. **Water-Limited Pattern:** In Metolius (Figure 3a), we observe that increase in K_{srad}^s and K_{sax} enhances HR, Tr, and GPP for all the combinations of specific root conductivities that are considered. Therefore, enhancements in K_{srad}^s and K_{sax} result in higher recirculation of moisture in the soil column together with higher transpiration and GPP for the entire set of combinations of K_{srad}^s and K_{sax} . This water-limited pattern was also observed in Blodgett.

3.1. Numerical Simulations

For each site, we base our simulation period on 1 or 2 years with the best available Ameriflux records that allow us to extract reliable forcing data and validate latent heat fluxes. The simulations performed are initialized with records of soil moisture when they are available, otherwise a spin-up is performed. We performed the spin-up using available information from years previous to those used in the simulations. For instance, at those sites where 2 years of information were unavailable, we use the same year twice for spin-up. Table 1 shows the information and years selected for each site for the initial conditions.

4. Results and Discussion

4.1. Root Hydraulic Conductivities and HR

In this study, we used a simplified approximation to compute the root surface and cross-sectional area (section 2.1). However, we observed that quantification of root areas is highly uncertain as

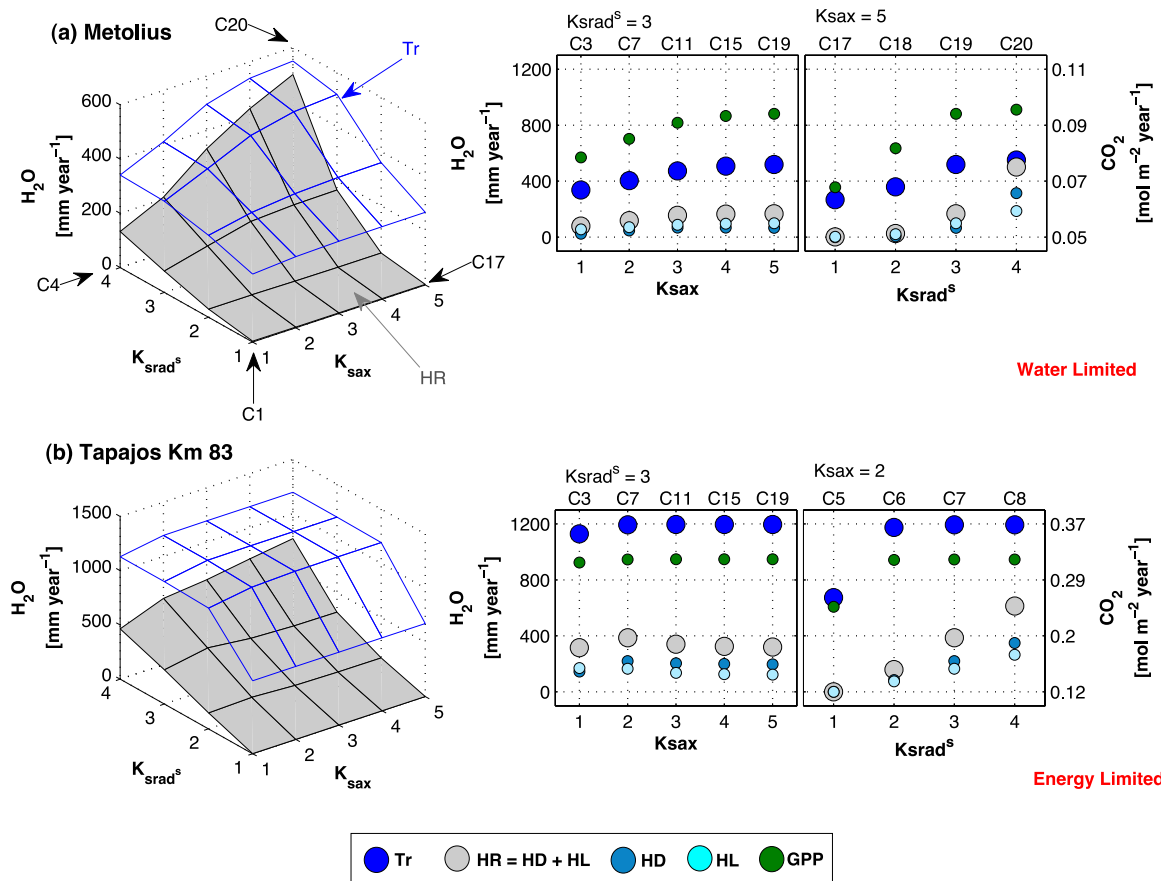


Figure 3. Effect of the saturated specific root radial hydraulic conductivity K_{srad}^s and the specific root axial conductivity K_{sax} on the fluxes of transpiration (Tr), hydraulic redistribution (HR), hydraulic lift (HL), hydraulic descent (HD), and gross primary production (GPP) at (a) Metolius Intermediate Forest and (b) Tapajós Km 83.

2. *Energy-Limited Pattern:* In Tapajós Km 83 (Figure 3b), we observe there is a water-limitation for low values of K_{srad}^s and K_{sax} . These low values are unable to support high transpirational fluxes. However, at the higher end there is a threshold after which a further increase in K_{srad}^s triggers a higher HR flux but it does not change Tr or GPP. After this threshold these sites are energy-limited. In other words, after this threshold higher K_{srad}^s and K_{sax} would enhance recirculation of moisture in the soil through HR but they are unable to enhance Tr and GPP. A similar pattern is observed in Harvard, Howland, Morgan, Willow Creek, and Duke.

4.2. Aboveground Dynamics

Figure 4 shows mean values of soil moisture (left plot) and mean diurnal fluxes of latent heat LE (right plot) for different combinations of specific root conductivities during the period of simulation, for Metolius and Tapajós Km 83 sites. In Metolius (Figure 4a), we observe that some combinations of specific conductivities are unable to reach the same fluxes recorded in the observations (e.g., C5), but also there are other combinations that result in fluxes of LE above those recorded at the tower (e.g., C16 and C20). Therefore, comparison with LE fluxes allows us to narrow the analysis and detect the combinations of specific conductivities that are able to match similar LE fluxes as the observations (e.g., C11, C12, C15, and C19). The same pattern is observed in the other water-limited site (Blodgett). In contrast, in Tapajós Km 83 (4b) we observe that low conductivities such as C5 are unable to predict the observed LE flux, but there is a threshold in the specific root conductivities above which all combinations of root conductivities above this threshold have the same patterns in LE fluxes, although they have different patterns in soil moisture. Figures for all the other sites are shown in supporting information Figure S4.

Comparison with LE fluxes is helpful to reduce the possible set of combinations and to be more confident about the fluxes of water that are leaving the soil. However, we observe that different combinations of root conductivities with rather different magnitudes of HR and different patterns of soil moisture may result in a

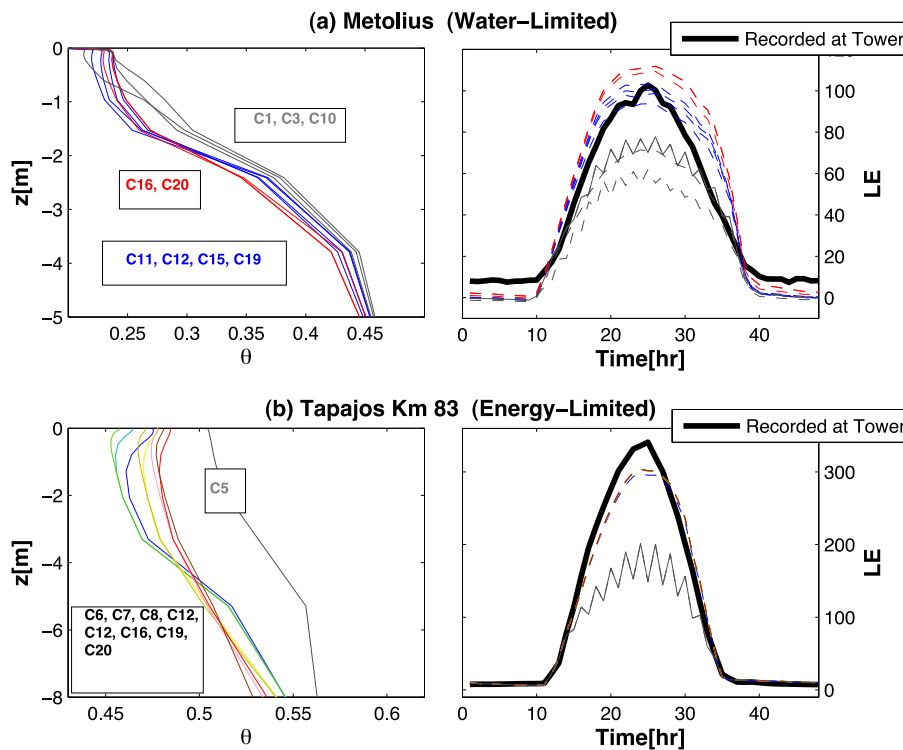


Figure 4. (left) Average soil moisture distribution in the soil domain and (right) mean diurnal latent heat fluxes for different combinations of root conductivities at (a) Metolius Intermediate Forest and (b) Tapajós Km 83.

similar outcome of LE that match the observations. This is more critical in the energy-limited sites and supports the claim by Neumann and Cardon [2012] implying that correct prediction of LE fluxes does not necessarily indicate that HR fluxes are correct. In turn, this suggests that aboveground validation is not sufficient to test the performance of numerical models for processes below the surface. In particular, overestimation or underestimation of HR could result in different distributions of soil moisture that reproduce the same dynamics above the ground.

4.3. Belowground Dynamics

Data of soil moisture measurements at different depths are available only for 4 of the 10 sites analyzed. These include: Tapajós Km 83, Metolius, Blodgett, and Willow Creek. It is worth to mention that simulations performed in this study are in one dimension and therefore computed fluxes are considered as an horizontal average, while the records of soil moisture are point measurements. As a result, we do not expect a perfect match between the soil moisture and the observations. Instead, the soil moisture observations are useful to analyze general patterns predicted by the model.

Figure 5 shows soil moisture in Metolius during 2006 at four different depths 10, 20, 30, and 70 cm, for combinations C11, C12, C15, and C19 which are the four combinations that resemble better the LE fluxes in Figure 4. Experimental records of soil moisture show diel patterns of soil moisture due to HR at all the different depths displayed in Figure 5. All the different combinations illustrated in Figure 5 are able to capture the general seasonal patterns in soil moisture and the diel patterns of HR. From Figure 3a, we see that annual fluxes of HR are significantly higher in C12 compared with C11, C15, and C19. Also in Figure 5, we observe that C12 slightly overestimates the diel patterns of HR. Therefore, we consider that combination C12 overestimates HR fluxes. However, from the soil moisture data are not possible to recognize which of C12, C15, and C19 is the most appropriate combination. The annual fluxes of HR in these combinations are on the same order of magnitude (Figure 3), and also the difference between these combination is only in K_{sax} .

There are two combinations (C11, C12) that match the LE patterns in Blodgett (supporting information Figure S4c). Figure 6 shows soil moisture in Blodgett during 2003 at two different depths, 10 and 30 cm. There is a clear and prominent HR diel pattern in the observations at 10 cm that becomes less evident at 30 cm.

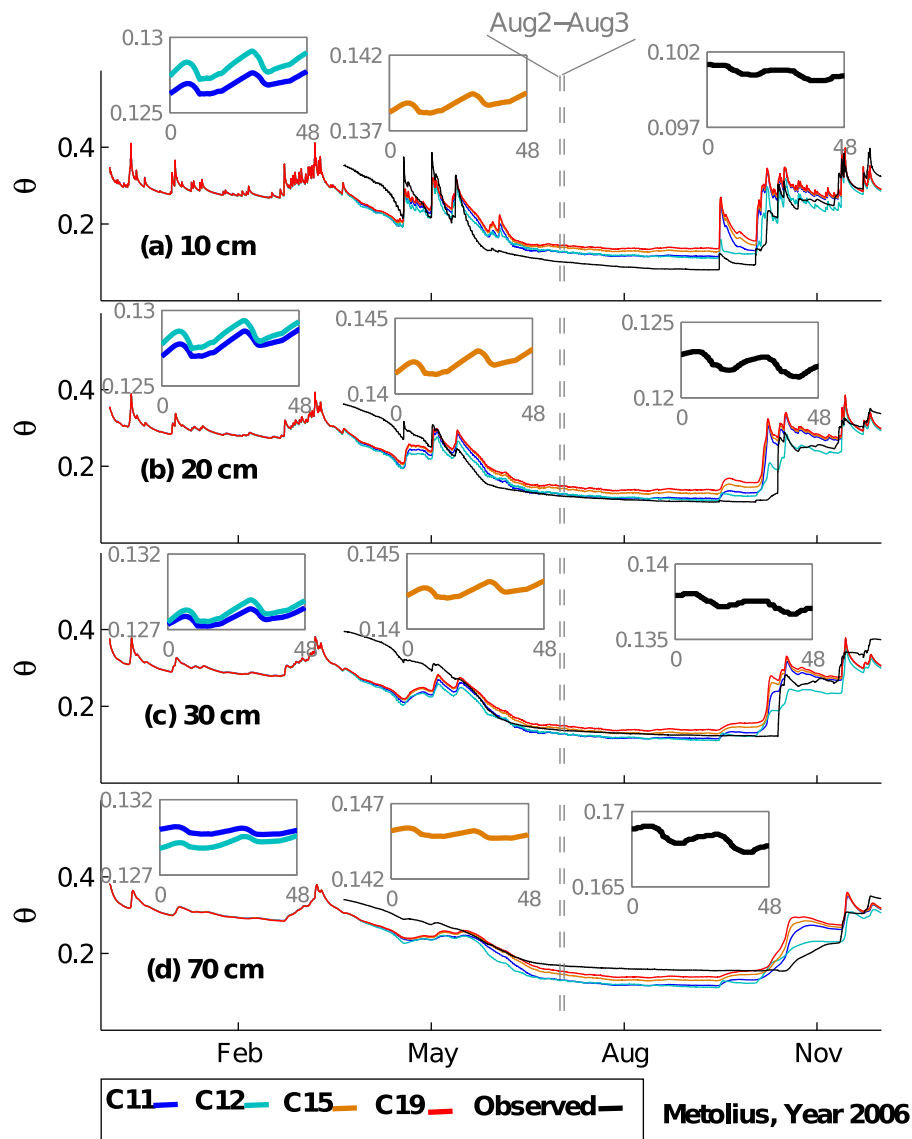


Figure 5. Soil moisture dynamics at Metolius Intermediate Forest at (a) 10 cm, (b) 20 cm, (c) 30 cm, and (d) 70 cm depth. The inset figures show the soil moisture dynamics in more detail for a period of 2 days corresponding to 2 and 3 August 2006.

Both combinations (C11, C12) are able to capture the general diel patterns of HR, however in combination C12 the diel patterns from the model are significantly more pronounced than from the data. Therefore, we conclude that C11 is the best selection for Blodgett site.

We observe in Figure 3b that combinations C1–C5 in Tapajós underestimate the LE fluxes. On the other hand, all the other combinations (C6–C20) reproduce similar patterns of LE fluxes. Figure 7 displays soil moisture in Tapajós Km 83 at four different depths during 2002. In this figure, four different combinations of root conductivities are displayed C5, C6, C7, and C8. There is a clear diel pattern of HR at 60 cm in the observations. However, HR signals are more sporadic at 15 and 30 cm, and disappear at 200 cm. We observe that combinations C6 and C7 are able to capture these general patterns of HR. However, there is a clear overestimation of HR fluxes in combination C8 that magnifies the diel patterns, and an underestimation in combination C5 that does not predict any diel HR pattern at all. Both C6 and C7 reproduce similar patterns and based on soil moisture and LE data both are equally appropriate.

In Willow Creek, we observe that combinations C1, C5, C9, C13, and C17 with the lowest K_{srad}^s underestimate the LE fluxes when compared with the observations (supporting information Figure S4d). All the

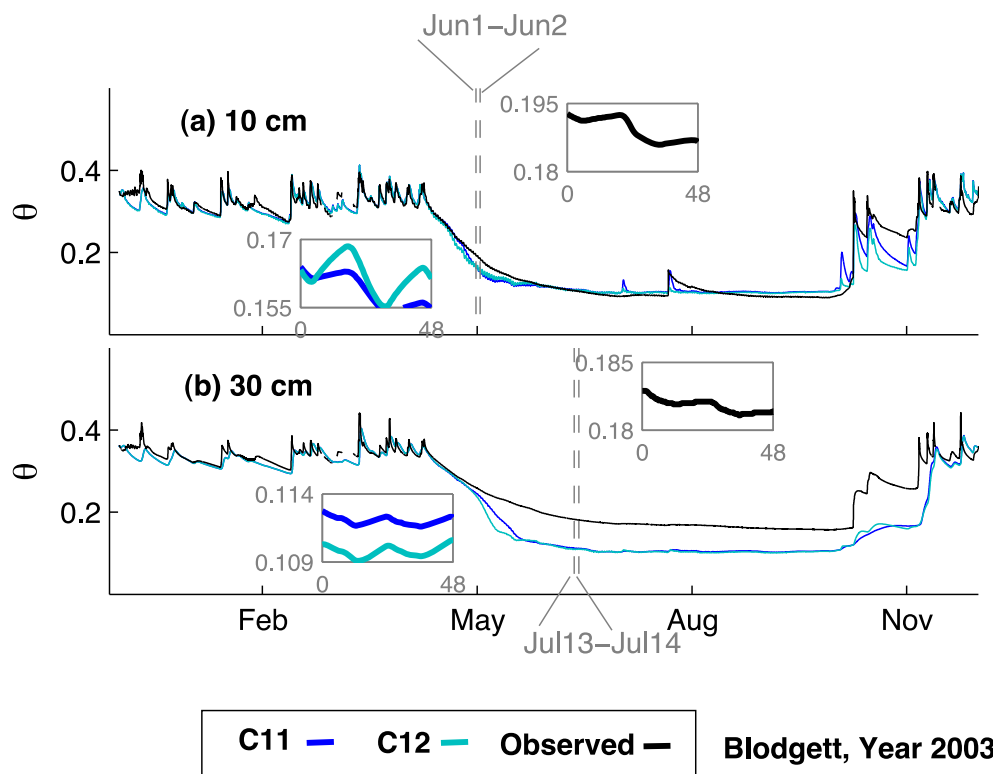


Figure 6. Soil moisture dynamics at Blodgett Forest at (a) 10 cm and (b) 30 cm depth. The inset figures show the soil moisture dynamics in more detail for a period of 2 days corresponding to (a) 1 and 2 June 2003 and (b) 13 and 14 July 2003.

other combinations predict very similar LE fluxes and are closer to the observations. Figure 8 shows soil moisture in Willow Creek at 10, 30, and 50 cm depth for simulations C2, C3, C6, and C7. Diel patterns of HR can be observed during sporadic dry periods at 10 and 20 cm depth. There are no HR patterns at 50 cm. We observe that combinations C2 and C6 capture the general patterns observed during these sporadic events. In contrast, combinations C3 and C7 overestimate the diel pattern of HR, and this is more critical at 10 cm. We conclude that both C2 and C6 present the best matching with available LE and soil moisture data.

4.4. Remarks

Comparison with LE fluxes and soil moisture suggests that in the water-limited ecosystems the best comparison of LE narrow the possible combinations of conductivities since few combinations are able to match the LE fluxes. In these sites, simulations with higher values of K_{srad}^s and K_{sax} result in overestimation of both LE and HR. On the other hand, simulations with lower values are unable to reach the same fluxes of LE reported by the flux net towers and to capture diel patterns of HR. In contrast, comparison with LE fluxes and soil moisture in energy-limited ecosystems suggested that several different combinations of K_{srad} and K_{sax} could result in similar patterns of LE, but with rather different fluxes of HR.

Comparison with available data of soil moisture helped us to analyze deeper the different combinations of root hydraulic conductivities. We were able to recognize diel patterns of HR at all the sites with available information of soil moisture. Although the frequency and amplitude of the diel patterns change across the four different sites we observe that:

1. High conductivities such as C20 results in overestimation of diel patterns of HR at all the sites. Similarly, low conductivities such as C1 or C5 were unable to capture the diel patterns of HR observed in the data.
2. Based on comparison with available data of soil moisture and LE, we see that combinations with the minimum values of K_{srad}^s and K_{sax} that resembles the fluxes of LE are a reasonable match for the diel pattern of HR observed in the soil moisture data.

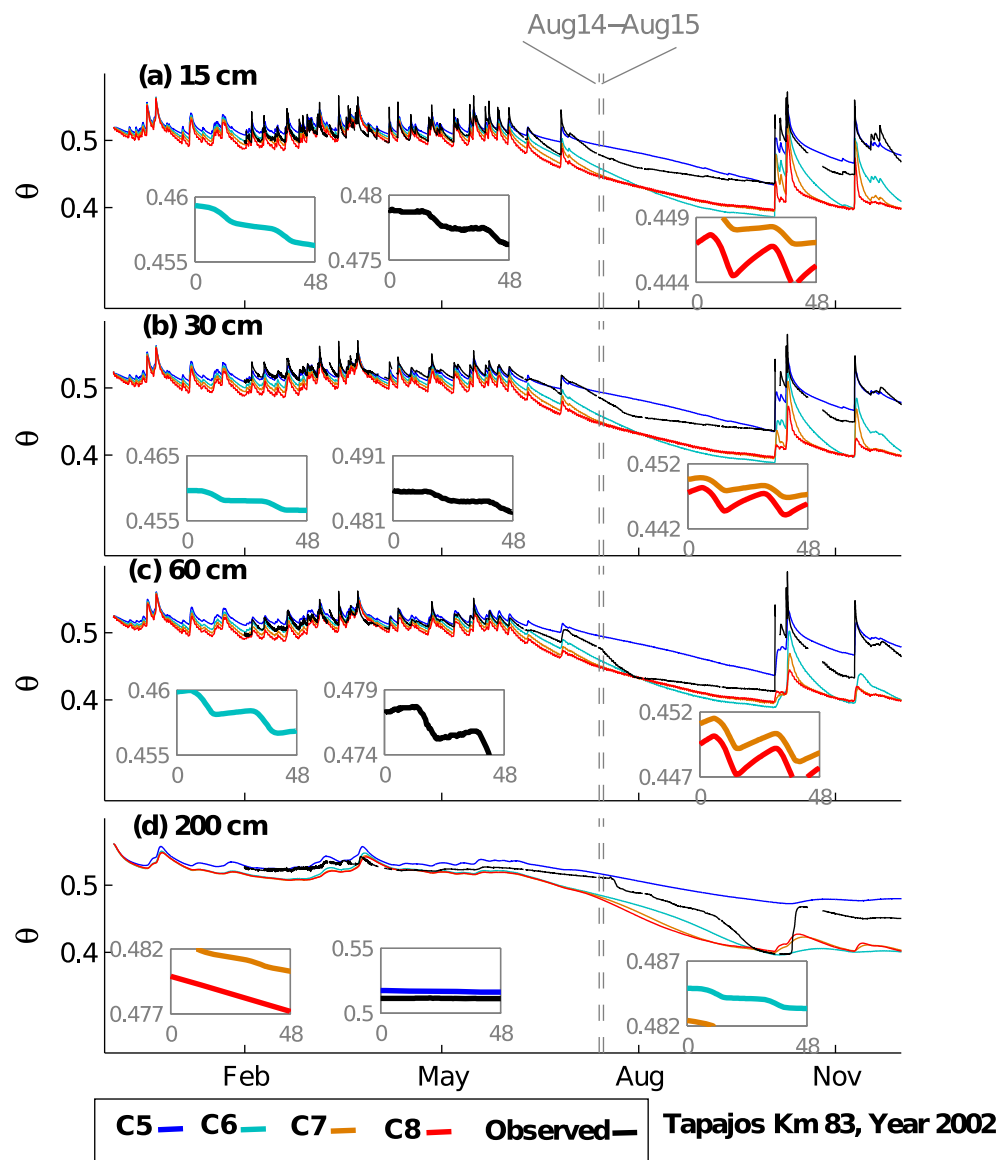


Figure 7. Soil moisture dynamics at Tapajós Km 83 at (a) 15 cm, (b) 30 cm, (c) 60 cm, and (d) 200 cm depth. The inset figures show the soil moisture dynamics in more detail for a period of 2 days corresponding to 14 and 15 August 2002.

5. Hydraulic Redistribution Patterns Across Different Climates

5.1. Soil Moisture Dynamics

Following the trends, we observe in the sites with available information of soil moisture we used the same criteria to select the most appropriate K_{srad}^s and K_{sax} in the other five sites where there are no available soil moisture measurements. Table 3 shows the most likely combination of K_{srad}^s and K_{sax} and the corresponding magnitude of HL, HD, and HR at all the different sites. Table 3 also shows the magnitude of HL, HD, and HR for combination C20, that includes the highest values of conductivities used in this study. Similarly, Figure 9 shows the corresponding dynamics of all the water fluxes across the period of simulation and for all the sites. Top plots show the incoming fluxes of SW radiation and PPT. Besides ET, several other components such as potential evapotranspiration (PET), HL, and HD are displayed. PET fluxes are computed using the Penman Monteith method, while all other fluxes are calculated using MLCan.

We can observe that the seasonal dynamics of HR can be explained through the dynamics of PET and PPT. HL occurs during high PET periods, and HD fluxes are high during PPT events after prolonged dry periods.

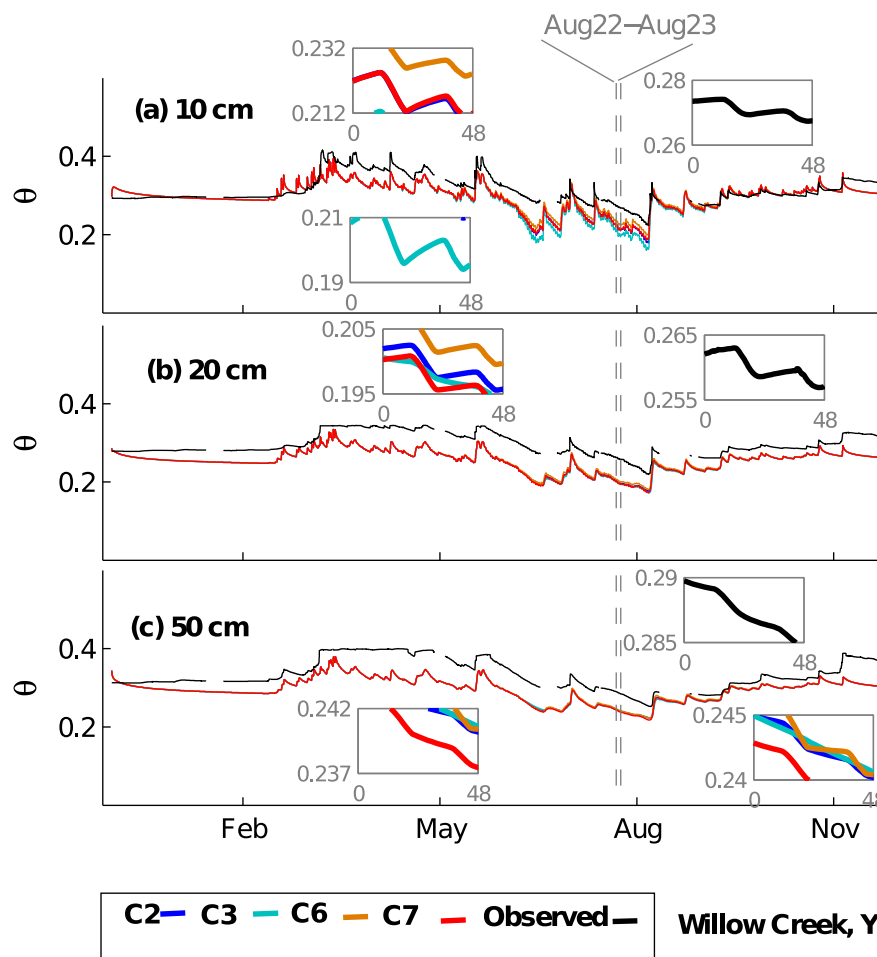


Figure 8. Soil moisture dynamics in Willow Creek at (a) 10 cm, (b) 20 cm, and (c) 50 cm depth. The inset figures show the soil moisture dynamics in more detail for a period of 2 days corresponding to 22 and 23 August 2001.

Although PET and PPT are able to explain general seasonal patterns associated with HR, the magnitude of HR varies significantly across the sites. Note that both Tr and PPT could be encapsulated in a single variable such as the soil moisture content θ ($\theta \propto \text{PPT} - \text{Tr}$). Therefore, the change of θ could be also connected with the magnitude of HR. Figure 9 shows the monthly normalized change of soil moisture $\delta\theta_m$ ($\delta\theta_m = \Delta\theta_m / \bar{\theta}_m$), where the net monthly change of soil moisture $\Delta\theta_m = (\theta_{\text{final}} - \theta_{\text{initial}})$ is normalized with respect to the mean monthly soil moisture $\bar{\theta}_m$. In other words, $\delta\theta$ estimates how significant is the monthly variation of moisture in the soil when it is compared with the actual available moisture in the soil column. We compute $\delta\theta$ for the entire soil column by performing a weighted average using the layer thickness. The soil depth considered here is that at which 95% of roots are located above it (z_{95}). In Figure 9, we observe that $\delta\theta_m$ reflects the seasonal dynamics of HR, with periods of HD associated with positive $\delta\theta_m$, and periods of HL associated with negative $\delta\theta_m$. However, note that the magnitude of HR fluxes is not being captured by the variation of $\delta\theta_m$. Therefore, the magnitude of HR is regulated not only by the net variation of water in the soil ($\Delta\theta$), but in particular how the soil moisture is distributed throughout the soil column. These results suggest that $\delta\theta_m$ could be used to infer the seasonal dynamics of HR under more simple simulations where the vertical distribution of moisture in the soil is not resolved, such as a bucket model. However, the distribution of soil moisture throughout the soil column is needed in order to capture the magnitude of HR fluxes.

5.2. Temperate Climate

Harvard, Howland, Morgan-Monroe, Willow Creek, and Duke receive a more homogeneous distribution of rainfall throughout the year, and experience a strong seasonal variation in SW radiation that impacts the

Table 3. Selected Combinations of Root Specific Conductivities K_{srad} and K_{sax} and Approximate Annual Fluxes Under These Simulations^{a,b}

Site	Best C	Most Likely Root Conductivity			Maximum HR (C20)			Previous Estimates ^c	
		HL (mm/yr)	HD (mm/yr)	HR/ET (%)	HL _{C20} (mm/yr)	HD _{C20} (mm/yr)	HR/ET _{C20}	Experimental Evidence	HR/ET (%)
AC	C2	10	3	1	54	128	30		
MET	C11–C15	87	68	32	93	157	68	[Brooks et al., 2002] Domec et al. [2004]	(35) ^d
					93				
BLO	C11	148	66	30	316	334	64		(35) ^e
HAR	C6	5	3	0.7	23	177	50		
HOW	C6	7	13	2	32	232	81		
DK	C14–C15	6	12	0.5–8	26	100	38		
MM	C10	10	3	2	61	203	48		
WC	C6–C7	2	2	1	20	108	35		
TAP67	C6–C7	44	52	4–16	213	555	96	Oliveira et al. [2005]	(8) ^g (3–30) ^f
TAP83	C6–C7	120	151	14–30	26	100	65	Oliveira et al. [2005]	(8) ^g (3–30) ^f

^aThe table also shows the annual fluxes under the highest combination of K_{srad} and K_{sax} (K20), and HR fluxes reported by previous studies.

^bSites: MET: Metolius Intermediate Pine, BLO: Blodgett, HAR: Harvard Forest, HOW: Howland, MOR: Morgan-Monroe, WC: Willow Creek, TAP: Tapajós Km 67 and Tapajós Km 83, AC: Austin Cary, DK: Duke.

^cThese estimates come from different sources and at different time scales.

^dBrooks et al. [2002].

^eSimulations with litter in Quijano et al. [2012, 2013].

^fPrevious Numerical Models reported in Neumann and Cardon [2012].

^gda Rocha et al. [2004].

fluxes of LE. The model predicts HR events during the summer period in all these sites. However, the summer period in these sites is associated with rainfall events that allow only short and sporadic dry periods that hampers HR fluxes. As a result the HR fluxes predicted by the model in these sites are significantly lower than those observed in Mediterranean climates (section 5.3). However, ecosystems experiencing continental climates with more prolonged dry periods, deeper roots, and different ecophysiological properties (e.g., higher stomatal conductance) may result in higher fluxes of HR as those we find in the sites considered here. For instance, Domec et al. [2010] pointed that HR fluxes in a loblolly pine plantation on the lower coastal plain of North Carolina presents significant higher fluxes of HR (HR/Tr ratios between 10 and 50%) than those observed in a similar loblolly plant plantation in Duke Forest (Ameriflux US-Dk3) where the soil depth is much shallower. In this study, the simulations for the hardwood plantation in Duke Forest (Ameriflux US-Dk2) with the same shallow soil predict also low fluxes of HR (HR/Tr ratios between 2 and 8%).

Figure 9a shows the simulation results in Austin Cary. This site experiences a warm temperate climate that is exposed to a more steady incoming SW radiation than the other temperate sites. The PPT at this site is accentuated during the summer period inducing a mild seasonality. Although there is a steady PET and also there is a seasonality in PPT, the fluxes of HR predicted by the simulations remain low all the year around. However, note that transpirational fluxes are much lower than Tapajós (Figures 9i and 9j). It seems the fluxes of Tr in Austin Cary are not large enough to compensate for the input of PPT and to create sufficient water potential gradients in the soil to trigger significant fluxes of HR.

5.3. Mediterranean Climate

In the Mediterranean climate sites of Metolius and Blodgett Forest, the lack of rainfall together with a high transpirational demand that is supplied to a large extent by deep roots enhances the fluxes of HL during the summer period. This pattern is illustrated in Figures 9b and 9c between June and September when HL fluxes are highest. On the other hand, the rainy season starts around October when Tr is reduced. During this period, the presence of rainfall events enhances the gradients of water potential triggering HD fluxes. There is experimental evidence of HR in *Pinus ponderosa* ecosystems in the Metolius River region of Oregon [Brooks et al., 2002; Domec et al., 2004]. In particular, Domec et al. [2004] observed that around 35% of water used for transpiration in the upper 2 m seemed to be replaced by HR during July and August. This pattern is similar to the simulations obtained here in Metolius where HL represented between 20 and 40% of Tr in July and August. However, Domec et al. [2004] reported no HR by the end of September. Although our

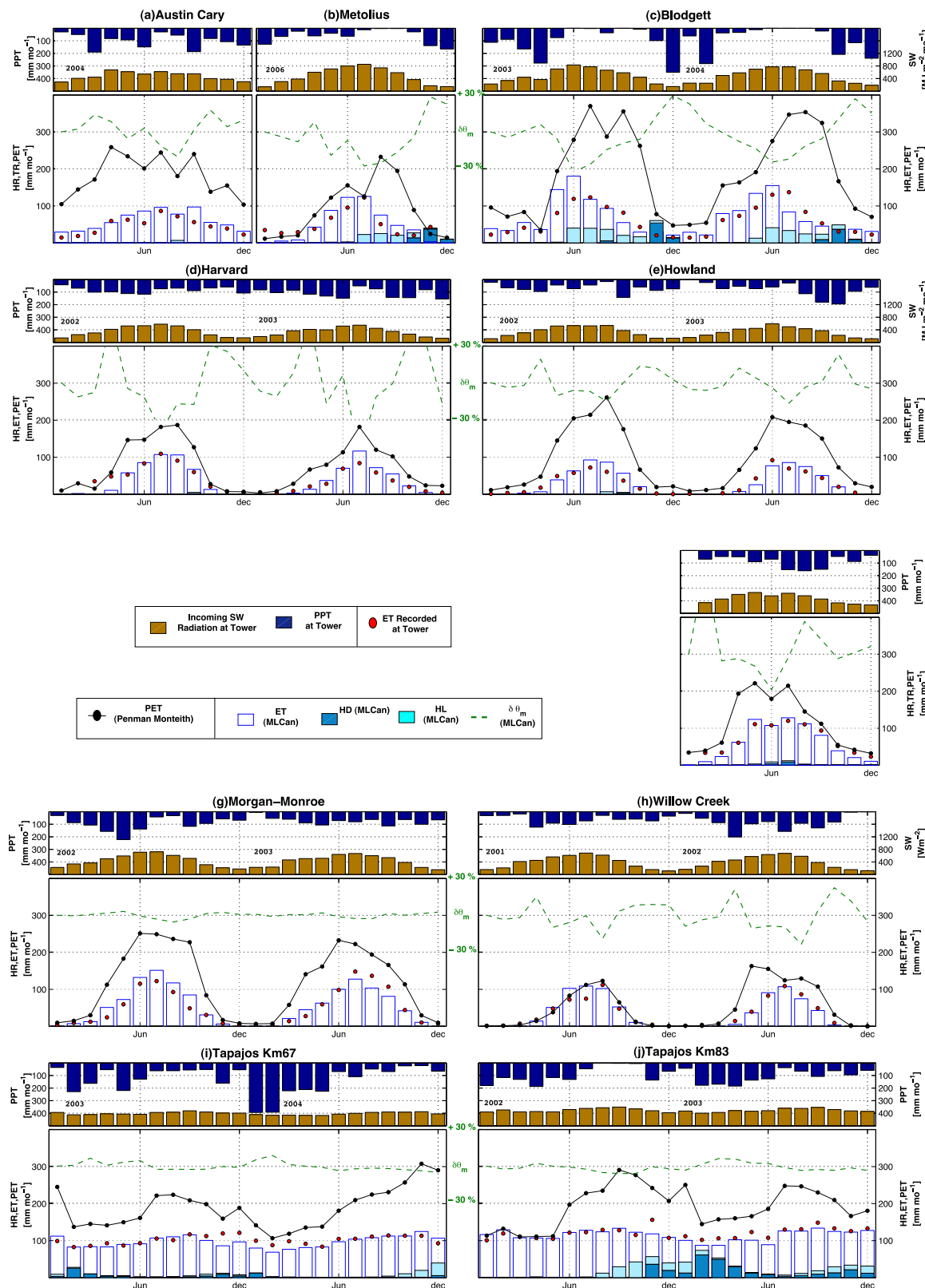


Figure 9. Simulations results for the eight study sites. Two plots are displayed for each site. (top) The annual patterns of precipitation and incoming shortwave radiation recorded by the flux towers, respectively. (bottom) The fluxes of evapotranspiration, hydraulic redistribution, hydraulic lift, and hydraulic descent from the simulations.

simulations show HL throughout September in Metolius, the transition from HL to HD was observed at the end of September where the fluxes of HL reduce significantly. HD fluxes become prominent in October and remain until the beginning of December. However, it is worth to mention that the study by Domec *et al.* [2004] was accomplished in 2002 while the simulations here in Metolius refer to 2006, and interannual variability in HR could be expected.

5.4. Tropical Moist Climate

Figures 9i and 9j show the simulation results for Tapajós Km 67 and Km 83, respectively. This tropical site experiences a strong dry period between June and November where the average monthly PPT is under 100 mm. Although there is a significant net reduction in PPT during the dry period the transpirational fluxes in Tapajós (Figures 9i and 9j) are distributed uniformly throughout the year. During the dry period, moisture is redistributed toward the surface from deeper layers through HL. However, this period is also associated with HD fluxes that are triggered by episodic PPT events. This presence of HL and HD makes the dry season at these sites different from the one observed in a Mediterranean climate (Figures 9b and 9c) where rainfall events are scarce or nonexistent and is dominated by HL. The uniform and constant pattern of ET flux that is observed in Tapajós is supplied from available moisture at different depths in the soil that enhances the gradients in water potential in the soil and drives HR. Although HD fluxes are triggered throughout the year, the highest fluxes of HD occur with the early rainfall events after dry periods which is the time when soil moisture is lowest. This is similar to the Mediterranean climate when the wet season arrives (Figures 9b and 9c).

Previous experimental studies have reported the presence of HR in the Amazon Forest [Oliveira *et al.*, 2005; da Rocha *et al.*, 2004]. In particular, Oliveira *et al.* [2005] based their work on the Floresta Nacional do Tapajós. They analyzed sap velocities in different trees and were able to recognize patterns of HL and HD in the critical transition between dry and wet periods. Figure 10 shows patterns of HL and HD with parameter combination C6 in Tapajós Km 67. In particular, diurnal patterns of HL and HD are contrasted with sap flow velocities reported by Oliveira *et al.* [2005] during January 2002 and August 2003. During the first days of January 2002 there is a clear pattern of HD in the model that is supported by negative values of sap velocities of tap roots in *Manilkara huberi*. Similarly, storm events during dry periods in August are associated with a transition from HL to HD that is supported by negative values of sap velocities of tap roots in *P. robustum* in Oliveira *et al.* [2005].

Both experimental and numerical data support the presence of HD and HL throughout the year in Tapajós driven by Tr and PPT patterns. Also, based on this comparison we see that our model is able to capture the general trends in HD and HL. However, quantification of the magnitude of HR fluxes in Tapajós where the root depth is around 10 m is challenging. In this study we observe that simulations C6 and C7 represent the best comparison with the available soil moisture and we conclude that annual ratios of HR/Tr range between 4 and 30% in Tapajós (see Table 3). Other studies have reported similar ratios [see Neumann and Cardon, 2012].

6. Conclusions

In this study, we have analyzed the dynamics of hydraulic redistribution (HR) by using data from 10 different Ameriflux sites that experience different seasonality of incoming shortwave radiation and precipitation. We have implemented the same numerical model for all these sites, and used a common parameterization. We were able to observe the presence of hydraulic redistribution in all the sites that were analyzed. However, the magnitude of the HR fluxes varies across the different sites and is controlled by different factors.

A major source of uncertainty in the magnitude of HR fluxes is the root hydraulic conductivities. We calculated the root hydraulic conductivities by performing a bottom-up scaling from isolated root measurements and performed a sensitivity analysis where different values of specific root hydraulic conductivities were considered based on ranges established in previous experimental studies. We found that specific root hydraulic conductivities impact significantly the magnitude of HR fluxes. In particular, the saturated specific root radial conductivity K_{srad}^s impacted the magnitude of HR at all the sites, and the specific root axial conductivity K_{sax} was mostly prominent in Mediterranean and tropical climates that experience long dry

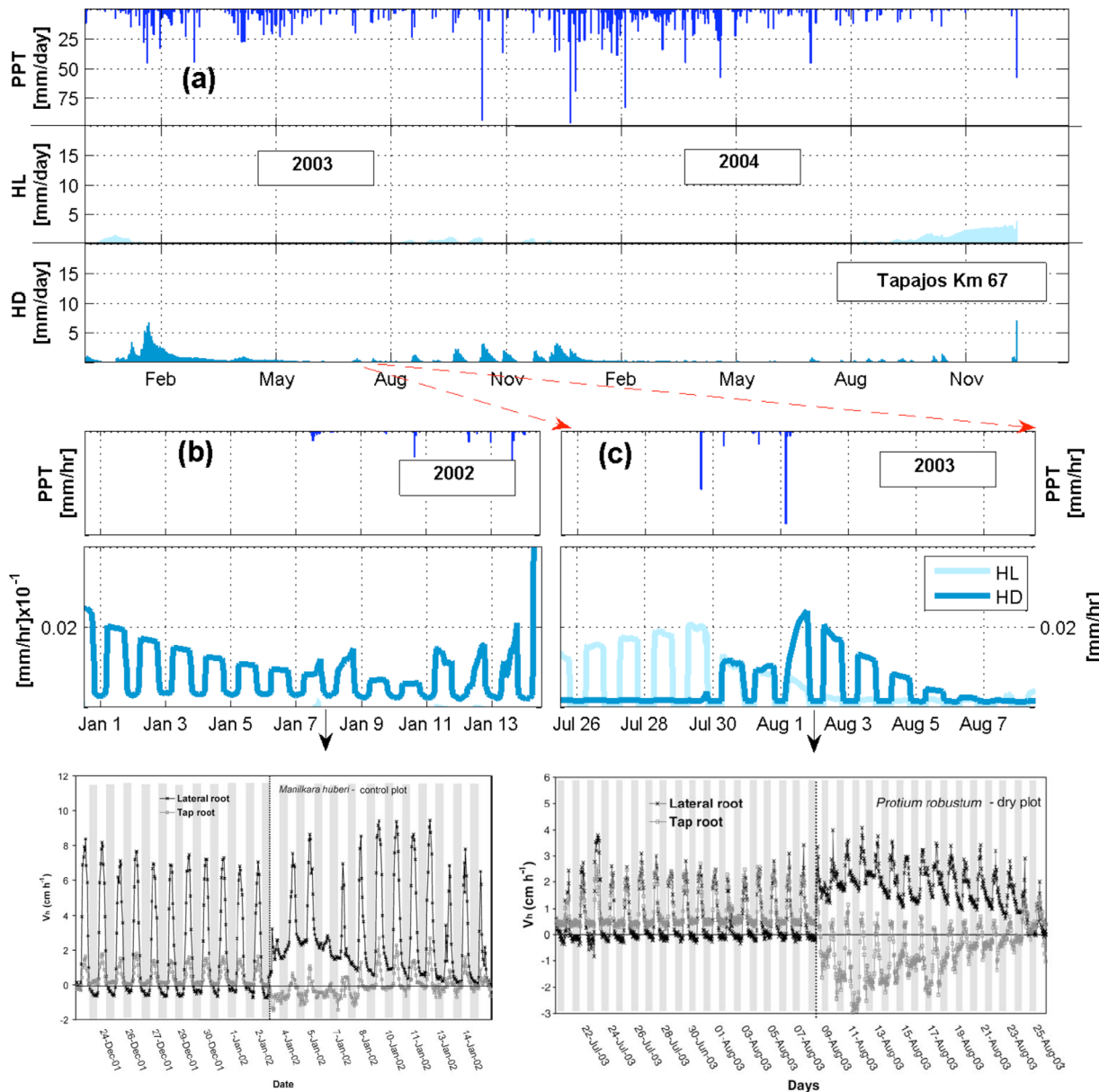


Figure 10. (a) Patterns of hydraulic lift (HL) and hydraulic descent (HD) during 2003 and 2004 in Tapajós Km 67 with simulation C6. HL and HD patterns are shown in more detail for the period of (b) January 2001, and (c) August 2003 that coincide with the period of experimental records reported by Oliveira *et al.* [2005]. Bottom figures show reported sap velocities in tap and lateral roots reported by Oliveira *et al.* [2005].

periods and deeper roots. Although both conductivities regulate the fluxes of transpiration (Tr) and HR we observed that, within the ranges of specific root conductivities that were selected, there was a higher sensitivity to K_{srad}^s . However, these results may be affected by inherent assumptions in the model that are ubiquitous in one-dimensional formulations such as the lack of lateral heterogeneity, the simplified approach of separating the complex root structure in only two major pathways (axial and radial), and the lack of water storage in the root system.

We observed that K_{srad}^s could enhance HR fluxes indefinitely while after some value there is no effect on Tr. In addition, we observed different responses to K_{srad}^s and K_{sax} across the different sites, which suggests that extrapolating root conductivities from one site to another as has been done in previous numerical approaches could induce errors in the quantification of HR. This may explain the cause of the discrepancy between previous modeling exercises and experimental studies reported by Neumann and Cardon [2012].

Parameters similar to K_{srad}^s can be found in all current models because it represents the ability of the root system to uptake or release moisture to the soil. For instance in the model developed by Ryel *et al.* [2002], the radial flow is controlled by the maximum radial conductance C_{RT} and a parameter c that reduces this conductance based on specific conditions; and in the model developed by Siqueira *et al.* [2008] the radial flow is controlled by the root membrane permeability K_r .

The selection of 10 different Ameriflux sites with available data of aboveground fluxes allows us to validate LE fluxes simulated by the model. However, we found that aboveground validation is not sufficient to test the performance of numerical prediction of HR fluxes. In energy-limited sites, we observed that different parameter combinations with rather different HR fluxes and soil moisture states could result in the same patterns of LE. Further comparison with available data of soil moisture in energy-limited sites confirm that high values of root specific hydraulic conductivities overestimate the diel pattern of HR observed in the soil moisture data.

Validation with both LE fluxes and soil moisture allowed us to select the most likely values of K_{srad}^s and K_{sax} and quantify the HR fluxes across the different climates. We found significant fluxes of HR in Mediterranean climates where strong seasonality triggers HL during the dry summer season and HD during the onset of the wet winter. We analyzed two different sites experiencing Mediterranean climates with rather different MAP and both present significant fluxes of HR. We also found significant fluxes of HR in tropical moist climates with prolonged dry periods such as Tapajós. In this case, HR fluxes are also triggered by a steady and prominent Tr flux that occurs all the year around. We observed a significant difference in HR fluxes between Tapajós with a tropical moist climate and Austin Cary with a warm temperate climate. Although both sites experience a uniform pattern of shortwave radiation throughout the year, the distribution of rainfall throughout the year is more homogeneous in Austin Cary with no extended dry periods, and lowers annual Tr. Finally, temperate climates with rainfall events distributed along the summer season hamper HR, resulting in fluxes close to 10 mm/yr. In this case, HR occurs only during dry events that occur sporadically across the summer season.

Since the first time HR was reported, it was associated as a mechanism that allows vegetation to enhance Tr and carbon uptake. Since then, several studies have quantified the effect of HR on Tr fluxes [Caldwell and Richards, 1989; Dawson, 1996; Ryel *et al.*, 2002; Lee *et al.*, 2005; Domec *et al.*, 2010] and have observed that HR enhances Tr in most of ecosystems although the net impact vary from site to site. However, further studies showed that HR can also be associated with several other processes such as ecological interactions [Dawson, 1993; Quijano *et al.*, 2012; Moreira *et al.*, 2003; Ludwig *et al.*, 2004], biogeochemical cycling [Quijano *et al.*, 2013; Armas *et al.*, 2011; Aanderud and Richards, 2009], and dynamics of microbial communities and fine roots in the soil [Querejeta *et al.*, 2003; Domec *et al.*, 2004]. However, the net impact of HR on these processes is directly associated with the magnitude of the water fluxes that are released in the soil. Based on the simulations performed in this study we observe that vegetation could enhance HR fluxes in all climates if specific root conductivities are increased. However, this will represent an additional cost of carbon for vegetation as it is directly associated with the root biomass. Analysis of available records of soil moisture and LE shows that the lowest values of root conductivities that are able to reproduce observed LE fluxes also provide good comparison with the soil moisture data. In contrast, we observe high values of root specific conductivities in energy-limited ecosystems maximize HR fluxes but show unrealistic diel patterns of soil moisture. As a result HR is negligible in some ecosystems such as those experiencing temperate climates with no prominent dry periods. This suggests that vegetation is investing in root conductivities to attain LE fluxes, but additional enhancements in root conductivities to maximize HR fluxes alone (with no additional enhancement of LE due to energy limitation) does not occur. Therefore, the additional benefits from HR (other than enhancing Tr) that have been observed are only important in sites experiencing dry periods, or the cost-benefit of investing in more root biomass (conductivities) to enhance HR is not worth after a given threshold.

Appendix A: Estimation of the Root Surface Area Index $A_{\text{ind},\text{sa}}$

Estimation of $A_{\text{ind},\text{sa}}$ is challenging, as it accounts for all the root surface area per unit of ground area, including coarse and fine roots and also mycorrhizal connection. Here as a first approximation, we estimate the surface area of coarse roots (diameter higher than 2 mm) from the basal area A_{basal} reported in the different

sites and by following the approach developed by *Noordwijk et al.* [1994] to compute the total root surface area from a proximal root. This approximation assumes the root system follows a fractal branching model. The surface area of coarse roots per unit of ground area is estimated as:

$$A_{\text{ind,sa,coarse}} = \sum_{i=0}^{N_p} A_{\text{sa},p} = \sum_{i=1}^{N_p} \{ N_p \pi d_p L_p \}. \quad (\text{A1})$$

where $A_{\text{sa},p}$ is the total root surface area in a given order p . The variables d_p , L_p , and N_p are the representative root diameter, root length, and number of roots for a given order p , respectively. N_p is the total number of orders in the root system. Note that the total number of elements in a given order can be determined from N_p and the branching number (N_k):

$$N_p = N_p^{N_k}. \quad (\text{A2})$$

The zero order ($p_k=0$) refers to the proximal root that here is assumed to have the same area as the basal area, and the maximum order (maxp) is computed such that $d_{\text{maxp}} = 2$ mm of diameter. Previous studies have reported relationships to link root and root diameter in different vegetation species [*Kalliokoski et al.*, 2008; *Ozier-Lafontaine et al.*, 1999]. Here we implemented this link based on previous approaches as:

$$L_p = 20 \cdot \log(d_p) + 60.75. \quad (\text{A3})$$

In order to quantify the root surface area of fine roots (diameter < 2 mm), we use estimates of fine roots surface area reported in *Jackson et al.* [1997]. Table 1 shows the surface area per unit of ground area of coarse roots ($A_{\text{ind,sa,coarse}}$), fine roots ($A_{\text{ind,sa,fine}}$), and total roots ($A_{\text{ind,sa}}$) for all the sites. $A_{\text{ind,sa}}$ is assumed to be distributed vertically following a logistic-dose function [*Schenk and Jackson*, 2002].

Acknowledgments

This research has been funded by NSF grants ATM 0628687, EAR 0911205, CBET 12091102, EAR 1331906, and EAR 1417444. JQ was also supported by the Dissertation Completion Fellowship 2012 from the University of Illinois at Urbana Champaign. The data for this paper are available at the Ameriflux data system. We acknowledge the following Ameriflux sites and their principal investigators for their data records: Metolius Intermediate Pine (PI: Beverly Law), Blodgett Forest (PI: Allen Goldstein), Harvard Forest (PI: J. William Munger), Duke Forest Hardwoods (PI: Ram Oren), Howland Forest Main (PI: David Y. Hollinger), Morgan-Monroe State Forest (PI: Kimberly Novick), Willow Creek (PIs: Paul Bolstad and Ankur Desai), LBA Tapajós Km 67 (PIs: J. William Munger, Scott R. Saleska, and Steven C. Wofsy), and Austin Cary (PI: Timothy A. Martin). In addition, funding for Ameriflux data resources was provided by the U.S. Department of Energy's Office of Science. We also would like to acknowledge the Oak Ridge National Laboratory (ORNL) Distributed Active Archive Center (DAAC), in particular the Large-Scale Biosphere-Atmosphere Experiment in the Amazon (LBA) project, for the continuous high-resolution frequency-domain reflectometry measurements of soil moisture to 10 m depth near each of the two towers located at the km 83 tower site (logged forest site) in the Tapajós National Forest in the state of Pará, Brazil.

Appendix B: Estimation of the Root Cross Area Index $A_{\text{ind,cs}}$

Computation of $A_{\text{ind,cs}}$ is challenging, especially for vegetation with deep root systems. However, this is an important variable that regulates the axial conductance of the root system. In this study, we calculate $A_{\text{ind,cs}}$ from information of basal area (A_{basal}) reported at each site (Table 1) and the root distribution. Note that $A_{\text{ind,cs}}$ at the surface is similar to A_{basal} . In addition, we assume that $A_{\text{ind,cs}}$ follows the same trend as the root distribution (see Figure 1). Therefore, in order to compute $A_{\text{ind,cs}}$ at each layer we consider that $A_{\text{ind,cs}}$ is proportional to the amount of roots at a given layer per unit of layer length. As a result, we are able to compute $A_{\text{ind,cs}}$ for the entire root system using the root distribution and the basal area. Thus, the magnitude of $A_{\text{ind,cs}}$ at a particular layer i in the soil domain can be computed as:

$$A_{\text{inc,cs}}^i = \frac{f_i}{\Delta z^i} \frac{\Delta z_1}{f_1} A_{\text{basal}}, \quad (\text{B1})$$

where f_i is the fraction of the total root biomass that is located in layer i .

References

- Aanderud, Z. T., and J. H. Richards (2009), Hydraulic redistribution may stimulate decomposition, *Biogeochemistry*, 95(2–3), 323–333, doi: 10.1007/s10533-009-9339-3.
- Amenu, G. G., and P. Kumar (2008), A model for hydraulic redistribution incorporating coupled soil-root moisture transport, *Hydrolog. Earth Syst. Sci.*, 12(1), 55–74.
- Armas, C., J. H. Kim, T. M. Bleby, and R. B. Jackson (2011), The effect of hydraulic lift on organic matter decomposition, soil nitrogen cycling, and nitrogen acquisition by a grass species, *Oecologia*, 168, 11–22.
- Baker, T. R., et al. (2004), Variation in wood density determines spatial patterns in Amazonian forest biomass, *Global Change Biol.*, 10(5), 545–562, doi:10.1111/j.1529-8817.2003.00751.x.
- Ball, J., and J. Berry (1982), The ci/cs ratio: A basis for predicting stomatal control of photosynthesis, *Year Book Carnegie Inst. Washington*, 81, 88–92.
- Brooks, J. R., F. C. Meinzer, R. Coulombe, and J. Gregg (2002), Hydraulic redistribution of soil water during summer drought in two contrasting Pacific northwest coniferous forest, *Tree Physiol.*, 22, 1107–1117.
- Burgess, S. S. O., M. A. Adams, N. C. Turner, and C. K. Ong (1998), The redistribution of soil water by tree root systems, *Oecologia*, 115(3), 306–311.
- Burgess, S. S. O., J. S. Pate, M. A. Adams, and T. E. Dawson (2000), Seasonal water acquisition and redistribution in the Australian woody phreatophyte, banksia prionotes, *Ann. Bot.*, 85(2), 215–224.
- Burgess, S. S. O., M. A. Adams, N. C. Turner, D. A. White, and C. K. Ong (2001), Tree roots: Conduits for deep recharge of soil water, *Oecologia*, 126(2), 158–165.

- Caldwell, M. M., and J. H. Richards (1989), Hydraulic lift—Water efflux from upper roots improves effectiveness of water-uptake by deep roots, *Oecologia*, 79(1), 1–5.
- Caldwell, M. M., T. E. Dawson, and J. H. Richards (1998), Hydraulic lift: Consequences of water efflux from the roots of plants, *Oecologia*, 113(2), 151–161.
- Christensen, N., and R. Peet (1984), Convergence during secondary forest succession, *J. Ecol.*, 72, 25–36.
- Clapp, R. B., and G. M. Hornberger (1978), Empirical equations for some soil hydraulic-properties, *Water Resour. Res.*, 14(4), 601–604.
- Curtis, P. S., P. J. Hanson, P. Bolstad, C. Barford, J. C. Randolph, H. P. Schmid, and K. B. Wilson (2002), Biometric and eddy-covariance based estimates of annual carbon storage in five eastern north American deciduous forests, *Agric. For. Meteorol.*, 113(1–4), 3–19, doi:10.1016/S0168-1923(02)00099-0.
- da Rocha, H. R., M. L. Goulden, S. D. Miller, M. C. Menton, L. D. V. O. Pinto, H. C. de Freitas, and A. M. e Silva Figueira (2004), Seasonality of water and heat fluxes over a tropical forest in eastern Amazonia, *Ecol. Appl.*, 14(4), supplement, S22–S32, doi:10.1890/02-6001.
- Dawson, T. E. (1993), Hydraulic lift and water use by plants: Implications for water balance, performance and plant-plant interactions, *Oecologia*, 95(4), 565–574.
- Dawson, T. E. (1996), Determining water use by trees and forests from isotopic, energy balance and transpiration analyses: The roles of tree size and hydraulic lift, *Tree Physiol.*, 16(1–2), 263–272.
- de Kroon, H., E. van der Zalm, J. W. A. van Rheenen, A. van Dijk, and R. Kreulen (1998), The interaction between water and nitrogen translocation in a rhizomatous sedge (*Carex flacca*), *Oecologia*, 116(1–2), 38–49, doi:10.1007/s004420050561.
- Domec, J. C., J. M. Warren, F. C. Meinzer, J. R. Brooks, and R. Coulombe (2004), Native root xylem embolism and stomatal closure in stands of douglas-fir and ponderosa pine: Mitigation by hydraulic redistribution, *Oecologia*, 141(1), 7–16.
- Domec, J.-C., J. S. King, A. Noormets, E. Treasure, M. J. Gavazzi, G. Sun, and S. G. McNulty (2010), Hydraulic redistribution of soil water by roots affects whole-stand evapotranspiration and net ecosystem carbon exchange, *New Phytol.*, 187(1), 171–83, doi:10.1111/j.1469-8137.2010.03245.x.
- Domingues, T. F., L. A. Martinelli, and J. R. Ehleringer (2007), Ecophysiological traits of plant functional groups in forest and pasture ecosystems from eastern Amazonia, Brazil, *Plant Ecol.*, 193, 101–112, doi:10.1007/s11258-006-9251-z.
- Drewry, D. T., P. Kumar, S. Long, C. Bernacchi, X.-Z. Liang, and M. Sivapalan (2010a), Ecohydrological responses of dense canopies to environmental variability. 1: Interplay between vertical structure and photosynthetic pathway, *J. Geophys. Res.*, 115, G04022, doi:10.1029/2010JG001340.
- Drewry, D. T., P. Kumar, S. Long, C. Bernacchi, X.-Z. Liang, and M. Sivapalan (2010b), Ecohydrological responses of dense canopies to environmental variability. 2: Role of acclimation under elevated CO₂, *J. Geophys. Res.*, 115, G04023, doi:10.1029/2010JG001341.
- Egerton-Warburton, L. M., J. I. Querejeta, and M. F. Allen (2008), Efflux of hydraulically lifted water from mycorrhizal fungal hyphae during imposed drought, *Plant Signal. Behavior*, 3(1), 68–71.
- Espeleta, J. F., J. B. West, and L. A. Donovan (2004), Species-specific patterns of hydraulic lift in co-occurring adult trees and grasses in a sandhill community, *Oecologia*, 138(3), 341–349.
- Ewers, B., D. Mackay, J. Tang, P. Bolstad, and S. Samanta (2008), Intercomparison of sugar maple (*Acer saccharum* marsh.) stand transpiration responses to environmental conditions from the western great lakes region of the United States, *Agric. For. Meteorol.*, 148(2), 231–246, doi:10.1016/j.agrformet.2007.08.003.
- Farquhar, G. D., S. V. Caemmerer, and J. A. Berry (1980), A biochemical-model of photosynthetic CO₂ assimilation in leaves of C-3 species, *Planta*, 149(1), 78–90.
- Frensch, J., and E. Steudle (1989), Axial and radial hydraulic resistance to roots of maize (*Zea mays* L.), *Plant Physiol.*, 91(2), 719–726.
- Huang, B. G., and P. S. Nobel (1994), Root hydraulic conductivity and its components, with emphasis on desert succulents, *Agron. J.*, 86(5), 767–774.
- Hultine, K. R., W. L. Cable, S. S. O. Burgess, and D. G. Williams (2003), Hydraulic redistribution by deep roots of a Chihuahuan desert phreatophyte, *Tree Physiol.*, 23(5), 353–360.
- Hultine, K. R., R. L. Scott, W. L. Cable, D. C. Goodrich, and D. G. Williams (2004), Hydraulic redistribution by a dominant, warm-desert phreatophyte: Seasonal patterns and response to precipitation pulses, *Funct. Ecol.*, 18(4), 530–538.
- Ishikawa, C. M., and C. S. Bledsoe (2000), Seasonal and diurnal patterns of soil water potential in the rhizosphere of blue oaks: Evidence for hydraulic lift, *Oecologia*, 125, 459–465.
- Jackson, R. B., H. A. Mooney, and E. D. Schulze (1997), A global budget for fine root biomass, surface area, and nutrient contents, *Proc. Natl. Acad. Sci. U. S. A.*, 94(14), 7362–7366.
- Kalliokoski, T., P. Nygren, and S. R. Sievanen (2008), Coarse Root Architecture of Three Boreal Tree Species Growing in Mixed Stands, *Silva Fennica* 42(2), 189–210, doi:10.14214/sf.252.
- Law, B. E., M. G. Ryan, and P. M. Anthoni (1999), Seasonal and annual respiration of a ponderosa pine ecosystem, *Global Change Biol.*, 5(2), 169–182.
- Le, P. V. V., P. Kumar, and D. T. Drewry (2011), Implications for the hydrologic cycle under climate change due to the expansion of bioenergy crops in the Midwestern United States, *Proc. Natl. Acad. Sci. U. S. A.*, 108(37), 15085–15090, doi:10.1073/pnas.1107177108.
- Le, P. V., P. Kumar, D. T. Drewry, and J. C. Quijano (2012), A graphical user interface for numerical modeling of acclimation responses of vegetation to climate change, *Comput. Geosci.*, 49, 91–101, doi:10.1016/j.cageo.2012.07.007.
- Lee, J. E., R. S. Oliveira, T. E. Dawson, and I. Fung (2005), Root functioning modifies seasonal climate, *Proc. Natl. Acad. Sci. U. S. A.*, 102(49), 17,576–17,581.
- Lopez, F. B., and P. S. Nobel (1991), Root hydraulic conductivity of 2 cactus species in relation to root age, temperature, and soil-water status, *J. Exp. Bot.*, 42(235), 143–149.
- Ludwig, F., T. E. Dawson, H. Kroon, F. Berendse, and H. H. T. Prins (2003), Hydraulic lift in acacia tortilis trees on an east African savanna, *Oecologia*, 134(3), 293–300.
- Ludwig, F., T. E. Dawson, H. H. T. Prins, F. Berendse, and H. Kroon (2004), Below-ground competition between trees and grasses may overwhelm the facilitative effects of hydraulic lift, *Ecol. Lett.*, 7(8), 623–631.
- McCulley, R. L., E. G. Jobbagy, W. T. Pockman, and R. B. Jackson (2004), Nutrient uptake as a contributing explanation for deep rooting in arid and semi-arid ecosystems, *Oecologia*, 141(4), 620–628.
- McFarlane, K. J., M. S. Torn, P. J. Hanson, R. C. Porras, C. W. Swanston, M. A. Callaham, Jr., and T. P. Guilderson (2013), Comparison of soil organic matter dynamics at five temperate deciduous forests with physical fractionation and radiocarbon measurements, *Biogeochemistry*, 112(1–3), 457–476, doi:10.1007/s10533-012-9740-1.
- Medlyn, B. E., et al. (1999), Effects of elevated [CO₂] on photosynthesis in European forest species: A meta-analysis of model parameters, *Plant Cell Environ.*, 22(12), 1475–1495, doi:10.1046/j.1365-3040.1999.00523.x.

- Melchior, W., and E. Steudle (1993), Water transport in onion (*Allium cepa* L.) roots—Changes of axial and radial hydraulic conductivities during root development, *Plant Physiol.*, 101(4), 1305–1315.
- Mendel, M., S. Hergarten, and H. J. Neugebauer (2002), On a better understanding of hydraulic lift: A numerical study, *Water Resour. Res.*, 38(10), 1183, doi:10.1029/2001WR000911.
- Misson, L., K. P. Tu, R. A. Boniello, and A. H. Goldstein (2006), Seasonality of photosynthetic parameters in a multi-specific and vertically complex forest ecosystem in the Sierra Nevada of California, *Trees Physiol.*, 26(6), 729–741.
- Miyamoto, N., E. Steudle, T. Hirasawa, and R. Lafitte (2001), Hydraulic conductivity of rice roots, *J. Exp. Bot.*, 52(362), 1835–1846, doi:10.1093/jexbot/52.362.1835.
- Moreira, M. Z., F. G. Scholz, S. J. Bucci, L. S. Sternberg, G. Goldstein, F. C. Meinzer, and A. C. Franco (2003), Hydraulic lift in a neotropical savanna, *Funct. Ecol.*, 17(5), 573–581.
- Neumann, R., and Z. Cardon (2012), The magnitude of hydraulic redistribution by plant roots: A review and synthesis of empirical and modeling studies, *New Phytol.*, 194(2), 337–352, doi:10.1111/j.1469-8137.2012.04088.x.
- Nobel, P. S., P. J. Schulze, and G. B. North (1990), Water influx characteristics and hydraulic conductivity for roots of *Agave deserti* Engelm, *J. Exp. Bot.*, 41(225), 409–415.
- Noordwijk, M., L. Spek, and P. Willigen (1994), Proximal root diameter as predictor of total root size for fractal branching models, *Plant Soil*, 164(1), 107–117, doi:10.1007/BF00010116.
- Oliveira, R. S., T. E. Dawson, S. S. O. Burgess, and D. C. Nepstad (2005), Hydraulic redistribution in three Amazonian trees, *Oecologia*, 145(3), 354–363, doi:10.1007/s00442-005-0108-2.
- Oren, R., B. Ewers, P. Todd, N. Phillips, and G. Katul (1998), Water balance delineates the soil layer in which moisture affects canopy conductance, *Ecol. Appl.*, 8(4), 990–1002, doi:10.2307/2640956.
- Ozier-Lafontaine, H., F. Lecompte, and J. Sillon (1999), Fractal analysis of the root architecture of *Gliricidia sepium* for the spatial prediction of root branching, size and mass: Model development and evaluation in agroforestry, *Plant Soil*, 209(2), 167–179, doi:10.1023/A:1004461130561.
- Pereira de Carvalho, J. O., J. N. Macedo Silva, and J. d. C. Alves Lopes (2004), Growth rate of a terra firme rain forest in Brazilian Amazonia over an eight-year period in response to logging, *Acta Amazonica*, 34(2), 209–217.
- Powell, T. L., G. Starr, K. L. Clark, T. A. Martin, and H. L. Gholz (2005), Ecosystem and understory water and energy exchange for a mature, naturally regenerated pine flatwoods forest in north Florida, *Can. J. For. Res.*, 35(7), 1568–1580, doi:10.1139/X05-075.
- Powell, T. L., H. L. Gholz, K. L. Clark, G. Starr, W. P. Cropper, and T. A. Martin (2008), Carbon exchange of a mature, naturally regenerated pine forest in north Florida, *Global Change Biol.*, 14(11), 2523–2538, doi:10.1111/j.1365-2486.2008.01675.x.
- Prieto, I., C. Armas, and F. I. Pugnaire (2012), Tansley review Water release through plant roots: New insights into its consequences at the plant and ecosystem level, *New Phytol.*, 193(4), 830–841, doi:10.1111/j.1469-8137.2011.04039.x.
- Querejeta, J., L. Egerton-Warburton, and M. Allen (2007), Hydraulic lift may buffer rhizosphere hyphae against the negative effects of severe soil drying in a California Oak savanna, *Soil Biol. Biochem.*, 39(2), 409–417.
- Querejeta, J. I., L. M. Egerton-Warburton, and M. F. Allen (2003), Direct nocturnal water transfer from oaks to their mycorrhizal symbionts during severe soil drying, *Oecologia*, 134(1), 55–64, doi:10.1007/s00442-002-1078-2.
- Quijano, J., P. Kumar, and D. T. D. Drewry (2012), Competitive and mutualistic dependences in vegetation dynamics enable by hydraulic redistribution, *Water Resour. Res.*, 48, W05518, doi:10.1029/2011WR011416.
- Quijano, J. C., P. Kumar, and D. T. Drewry (2013), Passive regulation of soil biogeochemical cycling by root water transport, *Water Resour. Res.*, 49, 3729–3746, doi:10.1002/wrcr.20310.
- Richardson, A. D., D. Y. Hollinger, D. B. Dail, J. T. Lee, J. W. Munger, and J. O. Keefe (2009), Influence of spring phenology on seasonal and annual carbon balance in two contrasting New England forests, *Tree Physiol.*, 29(3), 321–331, doi:10.1093/treephys/tpn040.
- Ryel, R. J., M. M. Caldwell, C. K. Yoder, D. Or, and A. J. Leffler (2002), Hydraulic redistribution in a stand of *Artemesia tridentata*: Evaluation of benefits to transpiration assessed with a simulation model, *Oecologia*, 130(2), 173–184.
- Schenk, H. J., and R. B. Jackson (2002), The global biogeography of roots, *Ecol. Monogr.*, 72(3), 311–328.
- Schmid, H. P., C. B. Grimmond, F. Cropley, B. Offerle, and H.-B. Su (2000), Measurements of $\{\text{CO}_2\}$ and energy fluxes over a mixed hardwood forest in the mid-western United States, *Agric. For. Meteorol.*, 103(4), 357–374, doi:10.1016/S0168-1923(00)00140-4.
- Schulze, E. D., M. M. Caldwell, J. Canadell, H. A. Mooney, R. B. Jackson, D. Parson, R. Scholes, O. E. Sala, and P. Trimborn (1998), Downward flux of water through roots (ie inverse hydraulic lift) in dry Kalahari sands, *Oecologia*, 115(4), 460–462.
- Scott, R. L., W. L. Cable, and K. R. Hultine (2008), The ecohydrologic significance of hydraulic redistribution in a semiarid savanna, *Water Resour. Res.*, 44, W02440, doi:10.1029/2007WR006149.
- Siqueira, M., G. Katul, and A. Porporato (2008), Onset of water stress, hysteresis in plant conductance, and hydraulic lift: Scaling soil water dynamics from millimeters to meters, *Water Resour. Res.*, 44, W01432, doi:10.1029/2007WR006094.
- Smith, D. M., N. A. Jackson, J. M. Roberts, and C. K. Ong (1999), Reverse flow of sap in tree roots and downward siphoning of water by *Grevillea robusta*, *Funct. Ecol.*, 13(2), 256–264.
- Tyree, M., and M. Zimmermann (2002), *Xylem Structure and the Ascent of Sap*, Springer-Verlag, Berlin Heidelberg, 284 pp., doi:10.1007/978-3-662-04931-0.
- Wang, G., C. Alo, R. Mei, and S. Sun (2011), Droughts, hydraulic redistribution, and their impact on vegetation composition in the Amazon forest, *Plant Ecol.*, 212(4), 663–673, doi:10.1007/s11258-010-9860-4.
- Warren, J. M., J. R. Brooks, F. C. Meinzer, and J. L. Eberhart (2008), Hydraulic redistribution of water from *Pinus ponderosa* trees to seedlings: Evidence for an ectomycorrhizal pathway, *New Phytol.*, 178(2), 382–394, doi:10.1111/j.1469-8137.2008.02377.x.
- Wayson, C. A., J. C. Randolph, P. J. Hanson, C. S. B. Grimmond, and H. P. Schmid (2006), Comparison of soil respiration methods in a mid-latitude deciduous forest, *Biogeochemistry*, 80(2), 173–189, doi:10.1007/s10533-006-9016-8.
- Wullschleger, S. D. (1993), Biochemical limitations to carbon assimilation in C 3 plants—A retrospective analysis of the j curves from 109 species, *J. Exp. Bot.*, 44(262), 907–920.
- Zhao, F., et al. (2011), Remote sensing of environment measuring effective leaf area index, foliage profile, and stand height in New England forest stands using a full-waveform ground-based lidar, *Remote Sens. Environ.*, 115(11), 2954–2964, doi:10.1016/j.rse.2010.08.030.